Research paper

Compounds that modulate AMPK activity and hepatic steatosis impact the biosynthesis of microRNAs required to maintain lipid homeostasis in hepatocytes

Jèssica Latorre[a,b,c,1], Francisco J. Ortega[a,b,c,1,*], Laura Liñares-Pose[d],
José M. Moreno-Navarrete[a,b,c], Aina Lluch[a,c], Ferran Comas[a,b,c], Núria Oliveras-Cañellas[a,c],
Wifredo Ricart[a,b,c], Marcus Höring[e], You Zhou[f,g], Gerhard Liebisch[e], P.A. Nidhina Haridas[h],
Vesa M. Olkkonen[h,i,1], Miguel López[d,1,**], José M. Fernández-Real[a,b,c,1,*]

[a] Institut d'Investigació Biomèdica de Girona (IDIBGI), Girona, Spain
[b] CIBER de la Fisiología de la Obesidad y la Nutrición (CIBEROBN), Madrid, Spain
[c] Department of Diabetes, Endocrinology and Nutrition (UDEN), Hospital of Girona "Dr Josep Trueta", Girona, Spain
[d] Department of Physiology, CiMUS, University of Santiago de Compostela, Instituto de Investigación Sanitaria, Santiago de Compostela, Spain
[e] Institute of Clinical Chemistry and Laboratory Medicine, Regensburg University Hospital, Regensburg, Germany
[f] Systems Immunity Research Institute, Cardiff University, Cardiff, United Kingdom
[g] Division of Infection and Immunity, Cardiff University School of Medicine, Cardiff, United Kingdom
[h] Minerva Foundation Institute for Medical Research, Biomedicum 2 U, Helsinki, Finland
[i] Department of Anatomy, Faculty of Medicine, University of Helsinki, Helsinki, Finland

ARTICLE INFO

ABSTRACT

Background: While the impact of metformin in hepatocytes leads to fatty acid (FA) oxidation and decreased lipogenesis, hepatic microRNAs (miRNAs) have been associated with fat overload and impaired metabolism, contributing to the pathogenesis of non-alcoholic fatty liver disease (NAFLD).
Methods: We investigated the expression of hundreds of miRNAs in primary hepatocytes challenged by compounds modulating steatosis, palmitic acid and compound C (as inducers), and metformin (as an inhibitor). Then, additional hepatocyte and rodent models were evaluated, together with transient mimic miRNAs transfection, lipid droplet staining, thin-layer chromatography, quantitative lipidomes, and mitochondrial activity, while human samples outlined the translational significance of this work.
Findings: Our results show that treatments triggering fat accumulation and AMPK disruption may compromise the biosynthesis of hepatic miRNAs, while the knockdown of the miRNA-processing enzyme DICER in human hepatocytes exhibited increased lipid deposition. In this context, the ectopic recovery of miR-30b and miR-30c led to significant changes in genes related to FA metabolism, consistent reduction of ceramides, higher mitochondrial activity, and enabled β-oxidation, redirecting FA metabolism from energy storage to expenditure.
Interpretation: Current findings unravel the biosynthesis of hepatic miR-30b and miR-30c in tackling inadequate FA accumulation, offering a potential avenue for the treatment of NAFLD.
Funding: Instituto de Salud Carlos III (ISCIII), Govern de la Generalitat (PERIS2016), Associació Catalana de Diabetis (ACD), Sociedad Española de Diabetes (SED), Fondo Europeo de Desarrollo Regional (FEDER), Xunta de Galicia, Ministerio de Economía y Competitividad (MINECO), "La Caixa" Foundation, and CIBER de la Fisiopatología de la Obesidad y Nutrición (CIBEROBN).

* Address for correspondence: FJ. Ortega, PhD.; JM Fernández-Real, MD., PhD. Section of Diabetes, Endocrinology and Nutrition (UDEN), Institut d'Investigació Biomèdica de Girona (IDIBGI), and CIBEROBN, Hospital "Dr. Josep Trueta" of Girona, Spain.
** M López, PhD. Department of Physiology, CiMUS, Instituto de Investigación Sanitaria de Santiago de Compostela, and CIBEROBN, University of Santiago de Compostela, Spain.
E-mail addresses: fortega@idibgi.org (F.J. Ortega), m.lopez@usc.es (M. López), jmfreal@idibgi.org (J.M. Fernández-Real).
[1] Equal contribution

1. Introduction

Non-alcoholic fatty liver disease (NAFLD) is characterized by the excessive build-up of fat in the liver parenchyma that is not caused by alcohol consumption. It is estimated to afflict around one billion individuals worldwide [1], and represents a spectrum of disturbances

Research in context

Evidence before this study

It is known that the excessive buildup of fat in the liver parenchyma is the basis for a spectrum of disturbances encompassing fatty acid (FA) infiltration (steatosis), which in turn leads to the activation of inflammatory pathways (steatohepatitis) related to the induction of impaired metabolism and insulin resistance. Together with circulating FA uptake, impaired β-oxidation occurring at the inner mitochondrial membrane, and de novo lipogenesis are of utmost importance for maintaining lipid homeostasis in hepatocytes, the most common parenchyma cells in liver. These processes are directly or indirectly modulated by the energy sensor AMP-activated protein kinase (AMPK), a master metabolic regulator that blocks the expression of lipogenic enzymes, while actively increases FA oxidation. Therefore, a number of AMPK-activating compounds have been reported to have beneficial effects as potential therapeutic interventions in the fatty liver arena. In particular, metformin, a common antidiabetic drug, can decrease hepatic steatosis by activating AMPK. Emerging evidence also suggests the involvement of key epigenetic modulators such as microRNAs (miRNAs). In this context, cell models may provide approaches to gain insight into the molecular mechanisms involved, and are important to the refinement of triggering factors and causal effectors in the field.

Added value of this study

In this study, we present results that deepen into the mechanisms underlying the relevance of miRNAs to de development of hepatosteatosis. Careful characterization of human hepatocytes challenged with different compounds disclosed the link between changes in AMPK activity, hepatic lipids and miRNA biosynthesis. Accordingly, while decreased hepatic miRNAs expression was coupled to enhanced de novo lipogenesis, transient transfection with specific miRNA candidates shortlisted the miR-30b and miR-30c as being capable of redirecting FA metabolism from energy storage to expenditure.

Implications of all the available evidence

The pathogenesis of non-alcoholic fatty liver disease (NAFLD) remains elusive and no effective therapy is available. Current results broaden our understanding of mechanisms of utmost importance for maintaining lipid homeostasis in hepatocytes, and unravel the activity of some hepatic miRNAs in tackling inadequate FA accumulation in liver, offering a potential avenue for the treatment of NAFLD.

protein kinase (AMPK), a master metabolic regulator that blocks the transcription of lipogenic enzymes [10], while actively inhibits biosynthetic pathways and increases FA oxidation [11]. Therefore, a number of AMPK-activating compounds have been reported to have beneficial effects as therapeutic interventions in the fatty liver arena [12,13]. In particular, metformin, a common antidiabetic drug, can decrease hepatic steatosis in rodent models by turning on AMPK [14–17]. Consistent with this notion, inhibition of AMPK leads to the activation of lipogenesis as a central event in the development of chemically-induced fatty liver [18]. In this context, the reagent called dorsomorphin or compound C, a pyrazolopyrimidine related to protein kinase inhibitors, is widely used as a cell-permeable ATP-competitive inhibitor of AMPK to revert the positive effects of AICAR and metformin [19,20]. On the other hand, exposure of hepatocytes to pathophysiologically relevant concentrations of palmitic acid results in the production of cytokines that also play an important role in the development of steatohepatitis [21]. These complementary approaches may provide insight into the molecular mechanisms involved in the multiple features of this complex condition, and are important to the refinement of triggering factors and causal effectors in the field [22].

MicroRNAs (miRNAs) are small non-coding RNAs that regulate gene expression by specific binding to complementary regions in coding messenger RNAs, leading to their translational repression or decay [23]. Since the coordination of a large number of genes may be accomplished by a single miRNA [24], these factors have become very attractive candidates to regulate cell fate decision in complex diseases [25]. In the context of impaired hepatic metabolism, the association between hepatic miRNAs and NAFLD is being increasingly recognized [26,27]. For instance, our previous transcriptional analysis in the liver of obese subjects disclosed decreased glucose metabolism and increased FA biosynthesis coupled to significant variations of specific hepatic miRNA species in subjects with this condition [28].

Here we investigated the expression of hundreds of mature miRNAs and genes related to fatty liver disease in primary human hepatocytes challenged by chemical compounds modulating steatosis, palmitic acid and compound C (as inducers), and metformin (as an inhibitor). By approaches performed both in vivo and in vitro, we confirmed that treatments triggering fat accumulation and AMPK disruption may compromise hepatic miRNA biosynthesis, while the knockdown of the miRNA-processing enzyme DICER exhibited a substantial increase in lipid deposition. Then, we validated consistent downregulation of specific hepatic miRNA candidates, pointing the loss of a few unique species at the forefront of the imbalance affecting de novo lipogenesis and FA uptake, oxidation and transport in hepatocytes, leading to the acquisition of NAFLD traits. Finally, transient transfection with mimic miRNA candidates shortlisted the miR-30b and miR-30c as being capable of redirecting FA metabolism from energy storage to expenditure, tackling inadequate FA accumulation in human hepatocytes.

2. Methods

2.1. Cell cultures

Primary human hepatocytes (HH) were grown on poly-L-lysine pre-coated dishes and cultured at 37 °C and 5% CO_2 atmosphere in hepatocyte medium supplemented with 5% fetal bovine serum (FBS), 100 units/ml penicillin and streptomycin (P/S), and 1% of a commercially available combination of different growth factors and hormones (Innoprot, Bizkaia, Spain). HepG2 cells were purchased from the American Type Culture Collection (ATCC) and cultured under same conditions in Dulbecco's Modified Eagle's Medium (DMEM) supplemented with 10% FBS, 100 units/ml P/S, and 1% glutamine and sodium pyruvate (Thermo Fisher Scientific, Wilmington, DE). Huh7 cells were cultured in Minimal essential Eagle Medium AQmedia™

encompassing fatty acid (FA) infiltration (steatosis), which often leads to the activation of inflammatory pathways (steatohepatitis) related to the induction of insulin resistance [2]. NAFLD is associated with obesity, hyperlipidemia, insulin resistance, type 2 diabetes, and a myriad of cardiovascular risk factors [3], being commonly described as the hepatic manifestation of metabolic syndrome [4,5]. Furthermore, NAFLD may precede more severe liver diseases such as cirrhosis and hepatocellular carcinoma [6].

The balance between FA biosynthesis, uptake and clearance is of utmost importance for maintaining lipid homeostasis in hepatocytes, the most common parenchyma cells in liver. Together with circulating FA intake, impaired β-oxidation occurring at the inner mitochondrial membrane [7], and de novo lipogenesis [8] substantially contribute to hepatic FA deposition [9]. All these processes are directly or indirectly modulated by the energy sensor AMP-activated

(Sigma-Aldrich, St. Louis, MO) with 10% FBS and 100 units/ml P/S. Decreased AMPK activity was induced by 10 μM compound C (CC). Exposure to 500 (HepG2) and 200 (HH) μM palmitic acid (PA) was accomplished as previously [28]. Transient AMPK activation was induced by 1 mM metformin (Sigma-Aldrich, St. Louis, MO). Each treatment was compared against the corresponding vehicle as control (*i.e.* 5% bovine serum albumin (BSA) for PA; 0.08% dimethyl sulfoxide (DMSO) for CC; and phosphate buffered saline (PBS) for metformin).

2.2. Silencing of hepatic AMPK in vivo

10-weeks old C57BL6 mice were held in a specific restrainer for intravenous injections Tailveiner (TV-150, Bioseb, France). Tail-injections were carried out using a 27 G X 3/8″ (0.40 mm x 10 mm) syringe. Mice were injected with either 100 μl of null (sh-luciferase) or AMPKα1-DN lentiviral particles in saline solution. The protein-coding sequence of AMPKα1-DN was cloned from pVQAd SF1-AMPKα1-DN (reference number: 24,603; ViraQuest Inc., North Liberty, IA) into the pSIN-Flag vector. To generate lentiviral particles, the pSIN-Flag vector containing AMPKα1-DN was co-transfected with packaging vectors (psPAX2 and pMD2G) into HEK293T, as previously [29]. psPAX2 and pMD2G vectors were a gift from Didier Trono (Addgene Plasmids, Cambridge, MA). These experiments were performed in agreement with the International Law on Animal Experimentation, and were approved by the USC Ethical Committee (Project ID 15,010/14/006).

2.3. Human liver samples

Sixty biopsy specimens were snap frozen in liquid nitrogen for genomic analyses and fixed in formalin for the histological assessment. Fixed samples were stained with hematoxylin-eosin and Masson's trichrome stain. All samples were evaluated by the same pathologist according to the degree of steatosis. Then, participants were stratified as subjects without significant steatosis (<5%), "borderline" (5−33%), and subjects with significant steatosis (>33% of fat). Exclusion criteria included cirrhosis or bridging fibrosis, a liver biopsy less than 2 cm long, and the use of statins. Gene and miRNA expression was performed as previously [28], using the commercially available TaqMan primer/probe sets (Applied Biosystems, Darmstadt, Germany) listed in the table of reagents provided as a **Supplemental file**. The study protocol was approved by the Ethics Committee and the Committee for Clinical investigation (CEIC) of the "Hospital Universitari dr. Josep Trueta de Girona". All subjects provided written informed consent before entering the study.

2.4. Depletion of AMPK and DICER in hepatocytes

Knockdown of AMPKα1/2 and DICER was performed by lentiviral particles expressing short hairpin (sh) interference RNA. HepG2 cells were plated, and 1:1 lentiviral particles were added for 24 h, together with 7 μg/ml polybrene. Stable clones were selected via puromycin dihydrochloride (Santa Cruz Biotechnology Inc., Dallas, TX).

2.5. In vitro transfection of mimic miRNAs

HepG2 and Huh7 cells were transfected for 48 h with 50 nM mimic miRNA candidates, or with a non-targeting (NT) miRNA control using HiPerfect Transfection Reagent (Qiagen, Gaithersburg, MD).

2.6. Genomic analysis

Total RNA was purified using the RNeasy Mini Kit (QIAgen, Gaithersburg, MD). Concentrations were assessed by a Nanodrop ND-1000 Spectrophotometer (Thermo Fisher Scientific, Wilmington, DE). Total RNA was reversed transcribed to cDNA using High Capacity cDNA Archive Kit (Applied Biosystems, Darmstadt, Germany). 600 ng of total RNA was used as input for miRNA reverse transcription by the TaqMan miRNA Reverse Transcription Kit, and TaqMan miRNA Multiplex RT Assays, as previously [30]. Expression of 754 mature miRNA species was assessed by means of TaqMan low-density arrays (Life Technologies, Darmstadt, Germany). Real-time PCR was carried out in a QuantStudio 7 Flex Real-Time PCR. Results were analysed with the QuantStudio™ Real-Time PCR Software (ThermoFisher Scientific). Commercially available TaqMan hydrolysis probes (Applied Biosystems, Foster City, CA) and forward/reverse SYBR Green® paired primers were used to analyze the expression of genes and miRNA candidates in a Light Cycler 480 II (Roche Diagnostics SL, Barcelona, Spain). SDHA (succinate dehydrogenase complex, subunit A) and PPIA (peptidylpropyl isomerase A), and RNU6b were used as endogenous controls for gene and miRNA expression, respectively. TaqMan assays and primers are listed in the **Supplemental file**. Complete miRNA profiles have been deposited in the community-endorsed repository Gene Expression Omnibus (GEO, http://www.ncbi.nlm.nih.gov/geo/, database with accession number GSE145039).

2.7. De novo lipogenesis

Transfected HepG2 cells were incubated for 3 h in complete media with 5 μCi/well of [³H]-Acetic acid (Amersham, GE Healthcare, Thermo Fisher Scientific Inc.). Total lipids were extracted as explained in reference [31]. Samples were run on thin layer silica-based chromatography using hexane/diethyl ether/acetic acid/water (65:15:1:0.25) as solvent. TAG, DAG and CE standards were run along with samples to identify the corresponding species. The three lipid species were scraped, and the [³H] radioactivity was measured by liquid scintillation counting. Results were normalized against total protein, determined by Pierce™ BCA Protein Assay Kit (Thermo Fisher Scientific, Wilmington, DE).

2.8. Lipidomics

Lipid extraction was performed as explained in reference [32]. The following lipid species were added as internal standards: PC 14:0/14:0, PC 22:0/22:0, PE 14:0/14:0, PE 20:0/20:0 (di-phytanoyl), PS 14:0/14:0, PS 20:0/20:0 (di-phytanoyl), PI 17:0/17:0, LPC 13:0, LPC 19:0, LPE 13:0, Cer d18:1/14:0, Cer 17:0, D7-FC, CE 17:0, and CE 22:0. The residues were dissolved in either 10 mM ammonium acetate plus methanol/chloroform (3:1, v/v) (for low mass resolution tandem mass spectrometry), or chloroform/methanol/2-propanol (1:2:4 v/v/v) with 7.5 mM ammonium formate (for high resolution mass spectrometry). The analysis of lipids was performed by direct flow injection analysis (FIA) using either a triple quadrupole mass spectrometer (FIA-MS/MS; QQQ triple quadrupole) [33,34] or a hybrid quadrupole-Orbitrap mass spectrometer (FIA-FTMS; high mass resolution) [35]. Lipid species were annotated according to the recently published proposal for shorthand notation [36]. Extracted data were processed by self-programmed Macros as described in [37]. Lipidomic data generated in this study have been made publicly available in Figshare [38] (10.6084/m9.figshare.11854563).

2.9. Mitochondrial oxygen consumption rate

The oxygen consumption rate (OCR) was measured in HepG2 transfected with mimic miRNAs by means of a Seahorse XF96 Extracellular Flux Analyser (Agilent Technologies, Santa Clara, CA). Cells were cultured for 48 h with transfection complexes, followed by 60 min of culture with XF base medium supplemented with 1 mM pyruvate, 2 mM glutamine, and 10 mM glucose in a CO_2 free incubator. The OCR was measured using the XF Cell Mito Stress Test Kit (Agilent Technologies, Santa Clara, CA). OCR was then normalized to the total protein content.

2.10. Quantification of apolipoprotein B100

Cell media were analysed using Human Apolipoprotein B ELISA[PRO] kit (3715−1HP-2, Mabtech, Sweden) according to the manufacturer's protocol. The absorbance was measured at 450 nm in a Cytation 5 Cell Imaging Reader (BioTek Instruments, Winooski, VT), and a 4-parameter curve fitting program was used for data analysis.

2.11. Triglyceride and cholesterol analysis

HepG2 cells transfected for 72 h with 100 nM mimic miRNA candidates or non-targeting miRNA control were subjected to triglyceride and cholesterol analysis using the GPO-PAP Triglyceride assay kit and the CHOD-PAP Cholesterol assay kit (Cobas, Roche/Hitachi, Tokyo, Japan). Data was normalized for total protein.

2.12. Prediction of miRNA target sites

Putative miRNA binding sites in 3′UTR messenger RNAs were assessed using TargetScan (http://www.targetscan.org), miRanda (http://www.microrna.org/), and miRWalk (http://zmf.umm.uni-heidelberg.de/apps/zmf/mirwalk2/). miRpath v.3 was employed to perform miRNA pathway analysis through experimentally validated miRNA interactions derived from DIANA-TarBase v6.0 [39]. Gene annotation enrichment analysis was performed by DAVID [40].

2.13. DNA constructs

Acyl-CoA synthetase long chain family member 1 (ACSL1) 3′UTR was amplified and inserted downstream of a firefly luciferase in the dual luciferase vector pEZX-MT06 (GeneCopoeia, Rockville, MD). Mutant ACSL1 3′UTR carrying a substitution of 7−8 nucleotides within the seed sequence of miRNA candidates was generated by oligonucleotide-directed PCR mutagenesis with Phusion[TM] High-Fidelity DNA Polymerase (Thermo Fisher Scientific, Wilmington, DE).

2.14. Luciferase assays

Huh7 cells were transfected for 48 h with the Luc-ACSL1 3′UTR wild-type or mutant constructs together with 200 nM mimic miRNAs by using Lipofectamine 2000[TM] (Invitrogen, Carlsbad, CA). Cell lysates were subjected to measurements of firefly and *Renilla* luciferase activities by using the Dual Luciferase Reporter Assay System (Promega, Madison, WI). Firefly signals were normalized by using the *Renilla* signal according to the manufacturer's instructions.

2.15. Lipid droplet staining

HepG2 and Huh7 cells were stained with 2 μM Bodipy 493/503 (Molecular Probes/Life Technologies, Eugene, OR). After washing, cover slips were mounted using Mowiol (Calbiochem, La Jolla, CA) containing 5 μg/ml DAPI (Thermo Scientific/Molecular Probes). Cells were imaged using Zeiss Axio Observer Z1 microscope (Carl Zeiss Imaging Solutions GmbH, Oberkochen, Germany), with the same exposure time for non-targeting control and mimic miRNAs. Staining was quantified using FIJI software (Image J) with a set cut-off threshold (total signal intensity/number of cells in the field). Treated and control HepG2 cells and primary HH were also fixed with paraformaldehyde 4%. Cells were dipped in 60% isopropanol before being stained with Oil Red O (Sigma, Lyon, France) for 10 min at room temperature. Absorbance was measured at 500 nm.

2.16. Western blot

Equal amounts of total protein were loaded on 10% SDS-PAGE. After separation, proteins were transferred onto Nitrocellulose (BioRad, Hercules, CA). Antibodies against ACSL1 (Abcam, Cambridge, UK), phospho and total AMPK, phospho and total ACC (Cell Signalling, Danvers, MA), and β-actin (Santa Cruz Biotechnology, Inc., Dallas, TX) were used. Blots were visualized by enhanced chemiluminescence (Thermo Fisher Scientific, Wilmington, DE) and signals were quantified by Image J software (https://imagej.nih.gov/ij/).

2.17. Statistics

Student's *t*-test, and One-Way ANOVA Post Hoc for Multiple comparisons by Fisher's Least Significant Difference (LSD) test (more than two groups) were performed to study differences between treatments. Associations between hepatic miRNAs and clinical outputs were determined by Spearman's. Data analyses were performed with SPSS v19.0 (IBM, Chicago, IL), GraphPad Prism 6 (Graphpad Holdings, LLC), and R Statistical Software (http://www.r-project.org/).

3. Results

3.1. Compounds that modify AMPK activity may compromise FA homeostasis

Our previous study established significant variations in primary human hepatocytes (HH) and HepG2 cells challenged with conditions that mimicked to some extent the onset of non-alcoholic fatty liver disease (NAFLD) [28]. Here, we performed further experimental approaches aimed at evaluating the impact of compounds that may compromise AMPK activity and fatty acid (FA) homeostasis in hepatocytes. For this, we exposed HH (Fig. 1a) and HepG2 cells (Fig. 1b) to palmitic acid (PA) and compound C (CC) as inducers, and to metformin (Mtf), which can mediate through or independently of AMPK-activation to alleviate fatty liver. First, we studied fat deposition (oil red O lipid-droplet staining) and the expression of genes related to *de novo* FA biosynthesis, uptake and transport, as well as altered expression of genes involved in glucose intake and inflammation. On one hand, treatments with PA and CC enhanced lipid accumulation in HH and HepG2 cells (Fig. 1a and Fig. 1b), and shortlisted increased *ACSL1* and *FASN* mRNA, while *GLUT2* expression was compromised in both HH and HepG2 cells (Fig. 1c and Fig. 1d). In parallel, the inflammatory activation was evident in hepatocytes challenged with PA, as suggested by enhanced expression of *IL8* (HH), *TNFα* (HepG2), and *ITGAX* (both). On the other hand, Mtf led to decreased lipid deposition (Fig. 1a and Fig. 1b), coupled to a significant downregulation of *ACSL1* in both cell models, decreased *FATP5* and *CD36* in HepG2 cells, and reduced *TNFα* in primary HH (Fig. 1c and Fig. 1d). Finally, we confirmed alterations in AMPK. As expected, both PA and CC disrupted AMPK activity in HepG2 (CC to a greater extent than PA), while Mtf significantly enhanced the phosphorylation of this kinase in both HH and HepG2 cells (Fig. 1e and Fig. 1f), thus increasing its activity. Altogether, these results confirmed chemically-induced molecular changes allowing lipid deposition in human hepatocytes, thus mirroring hepatosteatosis *in vitro*.

3.2. Compounds that compromise FA homeostasis also modulate miRNA biosynthesis

We used TaqMan Low Density Arrays (TLDA) to characterize the expression profile of 754 common mature microRNAs (miRNAs) in primary HH challenged with PA, CC, and Mtf. First, we identified hepatic miRNAs detectable in all samples (threshold Cts <35). *In vitro* cultured HH expressed as many as 226 miRNAs (~30%), with a substantial increase upon PA and Mtf (61.9% and 73%, respectively), and a striking downregulation accomplished by CC (63.7%, Fig. 2a). Indeed, compounds that led to significant alterations in AMPK activity and lipid deposition, modulating the expression of genes involved in FA metabolism, also modified the expression of several miRNAs,
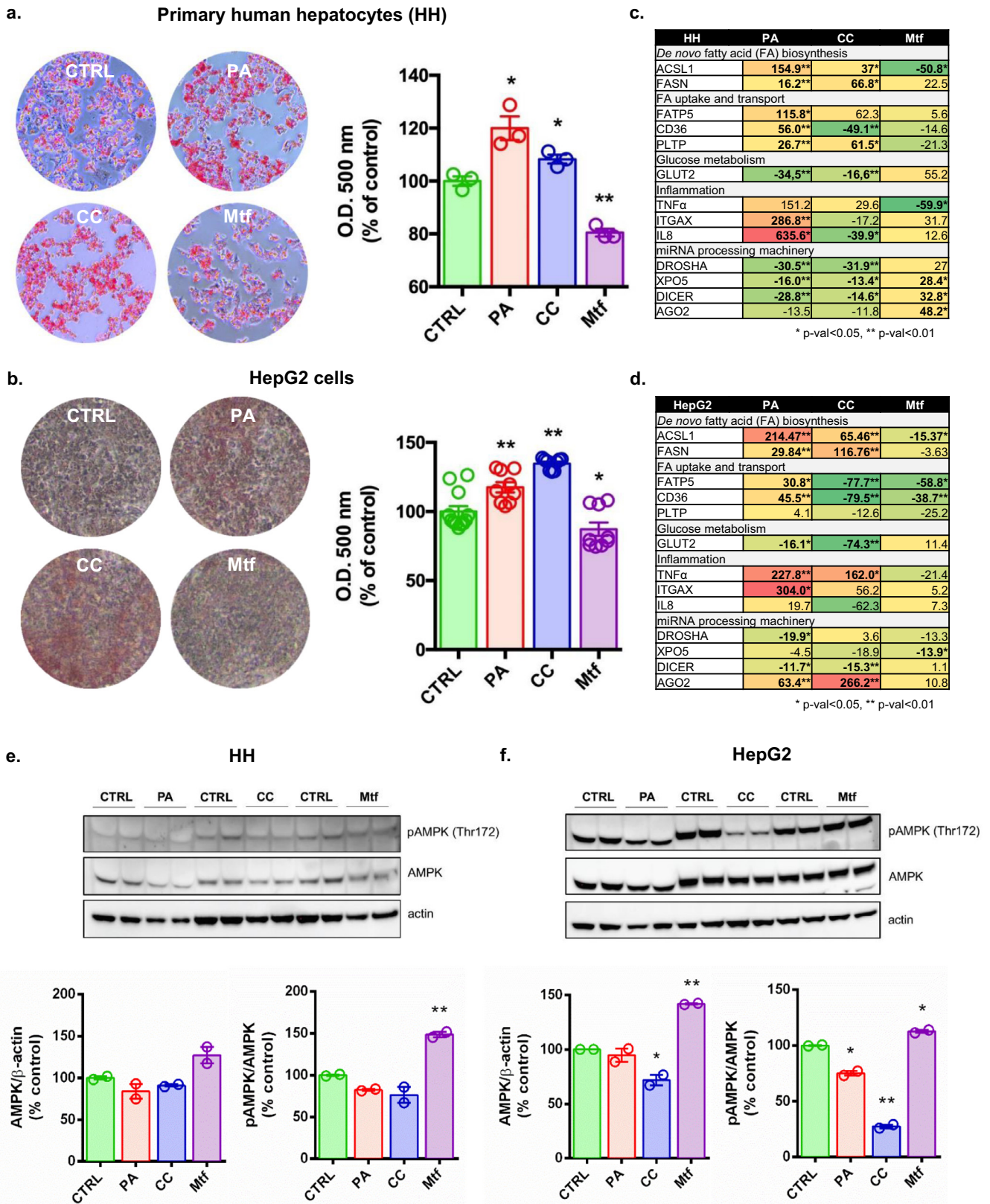
a. Primary human hepatocytes (HH)

c.

HH	PA	CC	Mtf
De novo fatty acid (FA) biosynthesis			
ACSL1	154.9**	37*	-50.8*
FASN	16.2**	66.8*	22.5
FA uptake and transport			
FATP5	115.8*	62.3	5.6
CD36	56.0**	-49.1**	-14.6
PLTP	26.7**	61.5*	-21.3
Glucose metabolism			
GLUT2	-34.5**	-16,6**	55.2
Inflammation			
TNFα	151.2	29.6	-59.9*
ITGAX	286.8**	-17.2	31.7
IL8	635.6*	-39.9*	12.6
miRNA processing machinery			
DROSHA	-30.5**	-31.9**	27
XPO5	-16.0**	-13.4*	28.4*
DICER	-28.8**	-14.6*	32.8*
AGO2	-13.5	-11.8	48.2*

* p-val<0.05, ** p-val<0.01

b. HepG2 cells

d.

HepG2	PA	CC	Mtf
De novo fatty acid (FA) biosynthesis			
ACSL1	214.47**	65.46**	-15.37*
FASN	29.84**	116.76**	-3.63
FA uptake and transport			
FATP5	30.8*	-77.7**	-58.8*
CD36	45.5**	-79.5**	-38.7**
PLTP	4.1	-12.6	-25.2
Glucose metabolism			
GLUT2	-16.1*	-74.3**	11.4
Inflammation			
TNFα	227.8**	162.0*	-21.4
ITGAX	304.0*	56.2	5.2
IL8	19.7	-62.3	7.3
miRNA processing machinery			
DROSHA	-19.9*	3.6	-13.3
XPO5	-4.5	-18.9	-13.9*
DICER	-11.7*	-15.3*	1.1
AGO2	63.4**	266.2**	10.8

* p-val<0.05, ** p-val<0.01

e. HH

f. HepG2

Fig. 1. Palmitate, compound C and metformin modify lipid deposition and AMPK activity in hepatocytes. Oil Red O staining in **a)** primary human hepatocytes (HH) and **b)** HepG2 cells challenged with palmitate (PA), compound C (CC) and metformin (Mtf), and control (CTRL). Optical density (OD) was measured and relative quantification of the Oil Red O staining is shown in plots. Charts show percent (%) of variation for gene expression measures obtained in treated **c)** HH and **d)** HepG2 cells *versus* respective vehicle as control. Color-scale goes from red (increased) to green (decreased). Western blots show results for phospho-AMPK (pAMPK, Thr172) and total AMPK in treated **e)** HH and **f)** HepG2 cells *versus* respective vehicle as control. pAMPK signal was computed relative to total AMPK, and total AMPK signal was normalized against β-actin. Results are expressed as mean $\pm$ SEM ($n \geq 2$ replicates/ cell/ treatment, * $p<0.05$, ** $p<0.01$ [Student t-test]).

with 30 miRNAs significantly decreased by CC, and 34 miRNAs significantly increased in hepatocytes challenged with Mtf (Fig. 2a). Such remarkable differences were observed in the context of 76 hepatic miRNAs with significant variations upon at least one of the treatments (Fig. 2b). Intriguingly, even though both PA and CC triggered lipid accumulation, quite few coincidences regarding miRNA deregulation were found between these two treatments in primary HH. Thus, we considered the opposite impact exercised by treatments of Mtf and CC as models of gain and loss of function, in reference to the activity of AMPK, significant changes in lipid deposition, and the opposite impact shown in miRNA patterns. Accordingly, together with miRNA hits linked to hepatosteatosis in a previous work [28], a final list of twelve miRNA candidates was validated on account of their consistent inverse expression patterns under these opposite conditions, significance upon normalization by different statistical approaches, *in silico* tools suggestive of their involvement in FA biosynthesis, and the high expression levels shown in HH (Cts <30). We then validated by qRT-PCR and individual TaqMan assays decreased expression of all these miRNA candidates upon CC, and the opposing pattern induced by Mtf for at least three of them: miR-30b, miR-146b, and miR-422a (Fig. 2c). In partial agreement, validation of miRNA hits in HepG2 confirmed significant downregulation of miR-26a, miR-30b, miR-30c, miR-34a, and miR-122 in cells challenged with either PA or CC, while reduced miR-29c, miR-146b, miR-222, and miR-422a accounted only upon PA treatment, and miR-16 and miR-139a were significantly decreased in HepG2 challenged with CC (Fig. 2c). Of note, Mtf treatment in HepG2 led to enhanced expression of miR-16 and miR-30b (Fig. 2c). Hence, treatments leading to impaired fat deposition and metformin-induced lipogenesis inhibition in HH and HepG2 cells appear to have a significant impact on miRNA regulation.

3.3. AMPK and DICER are required for the activity exercised by CC and MTF

As miRNA profiles in hepatocytes were so widely affected by treatments leading to significant changes in AMPK activity and lipid deposition, the expression of genes involved in miRNA biosynthesis was also investigated. Notably, decreased *DROSHA* and *DICER* in both HH and HepG2 cells upon PA and CC was further highlighted by the opposite upregulation exercised by Mtf in HH (Fig. 1c and Fig. 1d). As activation of the energy sensor AMP-activated protein kinase (AMPK, also known as *PRKAA1*) in hepatocytes drives FA oxidation and decreased lipogenesis, protecting against fatty liver disease [17], we aimed to investigate which mechanisms may underlie the observed effects through specific AMPK disruption. Thus, we assessed miRNA expression patterns and the metabolic commitment of cells subjected to *AMPK* knockdown. In agreement with our previous results, partial ablation of *AMPK* (−22.7%, *p* = 0.002 [ANOVA Post-Hoc LSD test]) resulted in increased lipid deposition (Fig. 3a) and enhanced expression of genes related to *de novo* lipogenesis (Fig. 3b). Given that chemical disruption of AMPK resulted in impaired expression of the miRNA-processing enzyme DICER, we sought to study whether this key regulator was also involved in the hepatic accumulation of FA. Thus, partial knockdown of *DICER* (−18.2%, *p* = 0.004 [ANOVA Post-Hoc LSD test]) was also accomplished in HepG2 cells, depicting similar effects as the knockdown of *AMPK*, including significant FA overload (Fig. 3a), and enhanced expression of *ACSL1, FASN*, and *CD36* (Fig. 3b). Accordingly, altered gene expression patterns were coupled to an overall miRNA downregulation, with consistent decrease of miR-26a, miR-29c, miR-30b, miR-34a, miR-146b, and miR-222 in both cell models (Fig. 3c). Thus, impaired *AMPK* and *DICER* gene expression and/or activity may play functional roles in decreased miRNA biosynthesis and the metabolic disruption affecting hepatic cells under conditions leading to increased FA deposition. To test this hypothesis, we evaluated the impact of CC and Mtf in *AMPK* and

DICER knockdown hepatocytes. The results show that under impaired *AMPK* gene expression neither treatments of CC nor Mtf were able to modulate lipid deposition in HepG2 cells (Fig. 3d). The lack of response to Mtf was apparent also at the gene expression level (Fig. 3e) and along many miRNA candidates (Fig. 3f). Thus, the positive impact of metformin through the regulation of specific hepatic miRNAs may depend to some extent on the expression of *AMPK* and, to a lesser extent, the expression of *DICER*.

3.4. AMPK modulation impacts hepatic miRNA biosynthesis in vivo

To further confirm the contribution of AMPK activity to miRNA regulation in liver we applied lentiviral particles harboring dominant negative isoforms of AMPKα (AMPK-DN) in the tail vein of mice. Significantly reduced levels of phospho-ACC were identified following the injection of lentiviral particles harbouring AMPK-DN, when compared to control (Fig. 4a). In keeping with the inhibition of liver AMPK and reduced phospho-ACC, increased hepatic lipid (Fig. 4b) and triglyceride content (Fig. 4c) were also detected. As expected, we found a marked increase in lipogenic genes such as *Acsl1* and *Fasn*, and decreased *Glut2* mRNA coupled to the significant downregulation of genes relevant for miRNA biogenesis, namely *Drosha* and *Ago2* (Fig. 4d). Notably, impaired *Ampk* expression also resulted in a significant deregulation of overall miRNA levels *in vivo* (Fig. 4e). Hence, current results *in vivo* strongly support our findings *in vitro*, linking impaired AMPK activity to hepatic miRNA biosynthesis.

3.5. Overexpression of miRNA candidates improves lipid metabolism

To assess whether impaired hepatic miRNA expression is at the forefront of changes in gene expression and the deposition of FA in hepatocytes, HepG2 and Huh7 cells were transfected with mimic miRNA or a non-targeting (NT) miRNA control. We found that, among our twelve miRNA candidates, only treatments with mimic miR-16, miR-30b, and miR-30c led to a significant reduction in the content and size of lipid droplets in hepatocytes (Fig. 5a). Accordingly, analysis performed by thin layer silica-based chromatography showed that the ectopic expression of these miRNA candidates drove reduced triglycerides, diacylglycerols, and cholesterol ester storage in transfected cells (Fig. 5b), while colorimetric assessment of triglycerides and cholesterols in the media verified a significant downregulation when hepatocytes were treated with mimic miR-30b or miR-30c (but not with miR-16) (Fig. 5c). Additionally, treatments with mimic miR-30b and miR-30c led to decreased apolipoprotein B (apoB) levels (Fig. 5d). Notably, quantitative analysis of the mitochondrial function (oxygen consumption rate, OCR) in HepG2 showed that cells transfected with mimic miR-30b and miR-30c accomplished 26% and 35% increase, respectively, while no significant change was found in human hepatocytes transfected with mimic miR-16 (Fig. 5e). Altogether, current results point out decreased lipid deposition and significant recovery of mitochondrial activity in human hepatocytes after transient transfection with mimic miR-30b and miR-30c.

3.6. Hepatic miRNA candidates regulate proteins that control FA storage

In silico analysis pointed at a variety of predicted target genes related to glucose and FA metabolism (Fig. 5f), many of which were experimentally tested. HepG2 cells transfected with mimic miR-16, miR-30b or miR-30c depicted decreased expression of genes coding for factors involved in the synthesis of triacylglycerols (Fig. 5g). Of note, expression of two genes directly related to the development of NAFLD, angiopoietin like 3 (*ANGPTL3*), a liver-secreted protein recently identified as a marker of NAFLD in mice and humans [41], and the membrane-bound O-acyltransferase 7 (*MBOAT7*), the disruption of which is related to liver disease [42], showed significant down and upregulation, respectively (Fig. 5g). In line with changes affecting
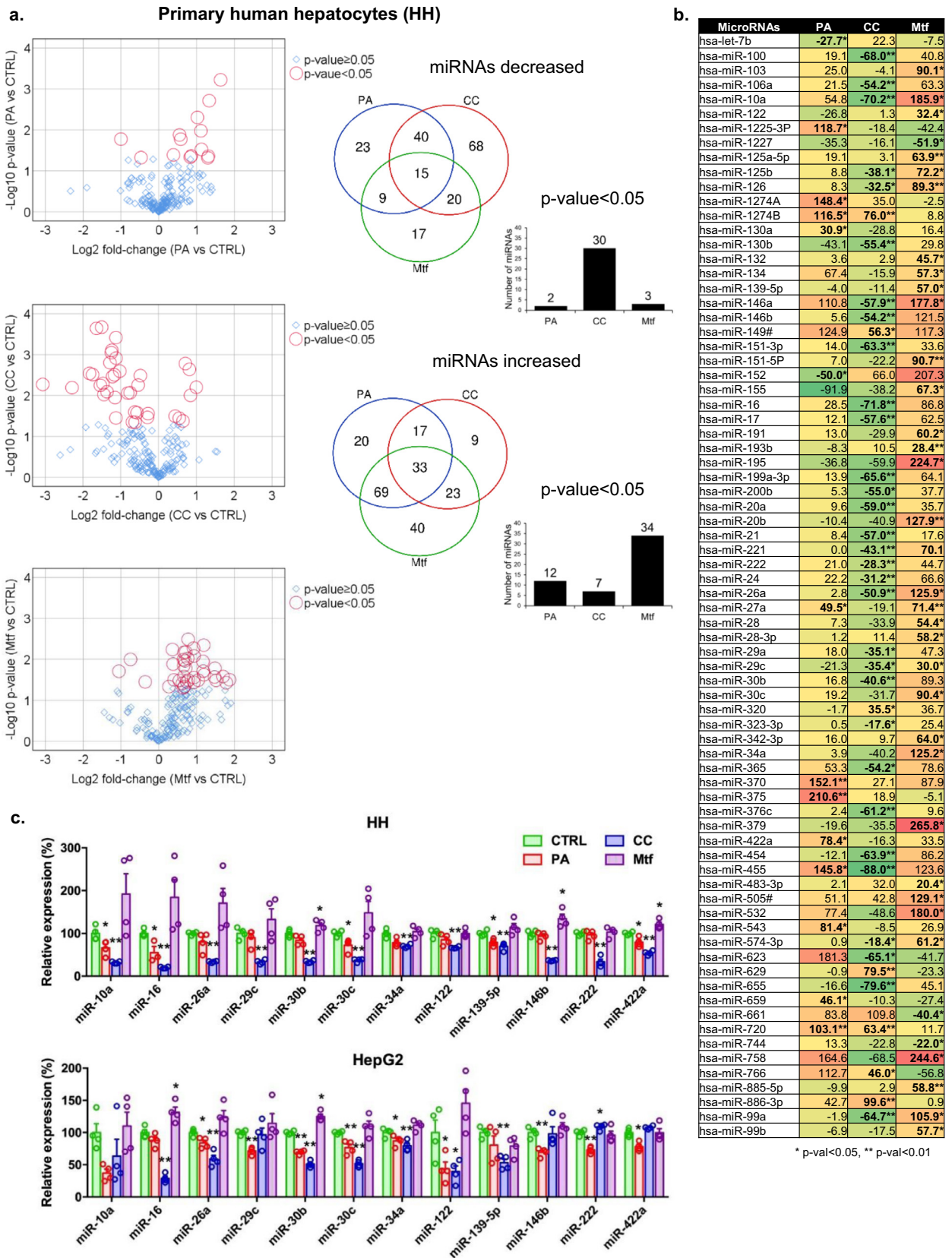
a.

Primary human hepatocytes (HH)

miRNAs decreased

p-value<0.05

miRNAs increased

p-value<0.05

b.

MicroRNAs	PA	CC	Mtf
hsa-let-7b	-27.7*	22.3	-7.5
hsa-miR-100	19.1	-68.0**	40.8
hsa-miR-103	25.0	-4.1	90.1*
hsa-miR-106a	21.5	-54.2**	63.3
hsa-miR-10a	54.8	-70.2**	185.9*
hsa-miR-122	-26.8	1.3	32.4*
hsa-miR-1225-3P	118.7*	-18.4	-42.4
hsa-miR-1227	-35.3	-16.1	-51.9*
hsa-miR-125a-5p	19.1	3.1	63.9**
hsa-miR-125b	8.8	-38.1*	72.2*
hsa-miR-126	8.3	-32.5*	89.3**
hsa-miR-1274A	148.4*	35.0	-2.5
hsa-miR-1274B	116.5*	76.0**	8.8
hsa-miR-130a	30.9*	-28.8	16.4
hsa-miR-130b	-43.1	-55.4**	29.8
hsa-miR-132	3.6	2.9	45.7*
hsa-miR-134	67.4	-15.9	57.3*
hsa-miR-139-5p	-4.0	-11.4	57.0*
hsa-miR-146a	110.8*	-57.9**	177.8*
hsa-miR-146b	5.6	-54.2**	121.5
hsa-miR-149#	124.9	56.3*	117.3
hsa-miR-151-3p	14.0	-63.3**	33.6
hsa-miR-151-5P	7.0	-22.2	90.7**
hsa-miR-152	-50.0*	66.0	207.3
hsa-miR-155	-91.9	-38.2	67.3*
hsa-miR-16	28.5	-71.8**	86.8
hsa-miR-17	12.1	-57.6**	62.5
hsa-miR-191	13.0	-29.9	60.2*
hsa-miR-193b	-8.3	10.5	28.4**
hsa-miR-195	-36.8	-59.9	224.7*
hsa-miR-199a-3p	13.9	-65.6**	64.1
hsa-miR-200b	5.3	-55.0*	37.8
hsa-miR-20a	9.6	-59.0**	35.7
hsa-miR-20b	-10.4	-40.9	127.9**
hsa-miR-21	8.4	-57.0**	17.6
hsa-miR-221	0.0	-43.1**	70.1
hsa-miR-222	21.0	-28.3*	44.7
hsa-miR-24	22.2	-31.2**	66.6
hsa-miR-26a	2.8	-50.9**	125.9*
hsa-miR-27a	49.5*	-19.1	71.4**
hsa-miR-28	7.3	-33.9	54.4*
hsa-miR-28-3p	1.2	11.4	58.2*
hsa-miR-29a	18.0	-35.1*	47.3
hsa-miR-29c	-21.3	-35.4*	30.0*
hsa-miR-30b	16.8	-40.6**	89.3
hsa-miR-30c	19.2	-31.7	90.4*
hsa-miR-320	-1.7	35.5*	36.7
hsa-miR-323-3p	0.5	-17.6*	25.4
hsa-miR-342-3p	16.0	9.7	64.0*
hsa-miR-34a	3.9	-40.2	125.2*
hsa-miR-365	53.3	-54.2*	78.6
hsa-miR-370	152.1**	27.1	87.9
hsa-miR-375	210.6**	18.9	-5.1
hsa-miR-376c	2.4	-61.2**	9.6
hsa-miR-379	-19.6	-35.5	265.8*
hsa-miR-422a	78.4*	-16.3	33.5
hsa-miR-454	-12.1	-63.9**	86.2
hsa-miR-455	145.8*	-88.0**	123.6
hsa-miR-483-3p	2.1	32.0	20.4*
hsa-miR-505#	51.1	42.8	129.1*
hsa-miR-532	77.4	-48.6	180.0*
hsa-miR-543	81.4*	-8.5	26.9
hsa-miR-574-3p	0.9	-18.4*	61.2*
hsa-miR-623	181.3	-65.1*	-41.7
hsa-miR-629	-0.9	79.5**	-23.3
hsa-miR-655	-16.6	-79.6**	45.1
hsa-miR-659	46.1*	-10.3	-27.4
hsa-miR-661	83.8	109.8	-40.4*
hsa-miR-720	103.1**	63.4**	11.7
hsa-miR-744	13.3	-22.8	-22.0*
hsa-miR-758	164.6	-68.5	244.6*
hsa-miR-766	112.7	46.0*	-56.8
hsa-miR-885-5p	-9.9	2.9	58.8**
hsa-miR-886-3p	42.7	99.6**	0.9
hsa-miR-99a	-1.9	-64.7**	105.9*
hsa-miR-99b	-6.9	-17.5	57.7*

* p-val<0.05, ** p-val<0.01

c.

Fig. 2. Palmitate, compound C and metformin impact miRNA expression patterns in hepatocytes. **a)** Volcano plots represent changes in miRNA expression profiles assessed in primary human hepatocytes (HH) challenged with palmitate (PA), compound C (CC) and metformin (Mtf). Red circles stand for statistically significant miRNAs ($p<0.05$). Venn diagrams plot the number of decreased/ increased miRNA upon treatments with PA (blue), CC (red) and Mtf (green). The number of hepatic miRNAs with significant alteration is depicted in the bar plots. **b)** Statistically significant variations detected in miRNA quantities for at least one of the treatments. Color-scale goes from red (increased) to green (decreased). **c)** TaqMan assessment and expression levels of preselected miRNA hits in both HH and HepG2. Results are expressed as mean ± SEM ($n \geq 3$ replicates/ cell/ treatment, * $p<0.05$, ** $p<0.01$ [Student *t*-test]).
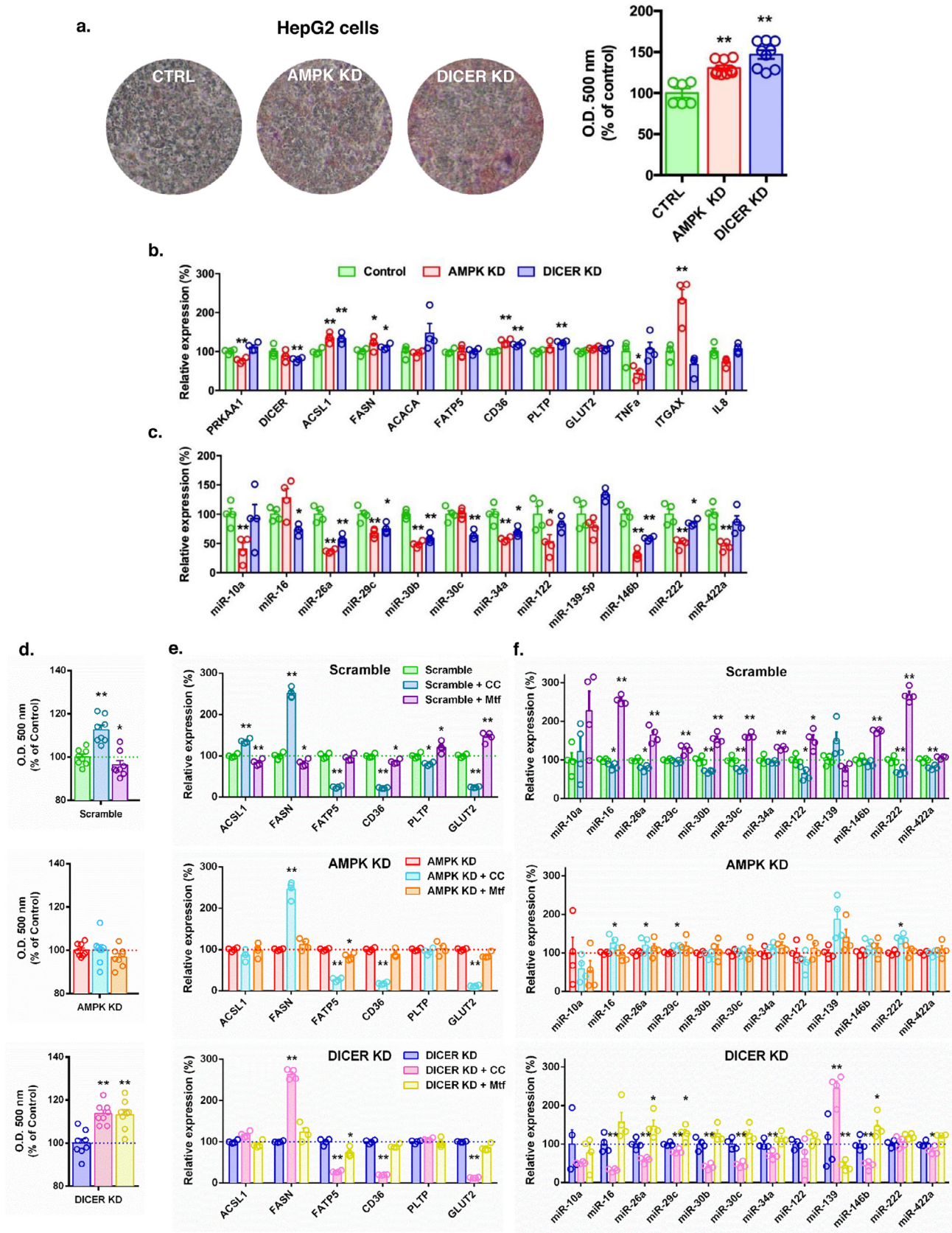
Fig. 3. *AMPK* and *DICER* knockdown enhances lipid accumulation in hepatocytes. **a)** Oil Red O staining of *AMPK* and *DICER* knockdown (KD), and control HepG2 cells transfected with lentiviral negative control vector containing scrambled sh-RNA (CTRL). Optical density (O.D.) was measured at 500 nm. **b)** Gene expression and **c)** miRNA hits assessed in *AMPK* (a.k. a. *PRKAA1*) and *DICER* KD *versus* scrambled control cells. **d)** Impact of compound C (CC) and metformin (Mtf) on **d)** measures of Oil Red O staining, **e)** gene expression patterns, and **f)** miRNA candidates in sh-RNA scrambled, *AMPK* KD and *DICER* KD hepatocytes. Results are expressed as mean ± SEM (* $p < 0.05$, ** $p < 0.01$ [One-Way ANOVA corrected for multiple comparisons by the Fisher's least significant difference (LSD) test]).
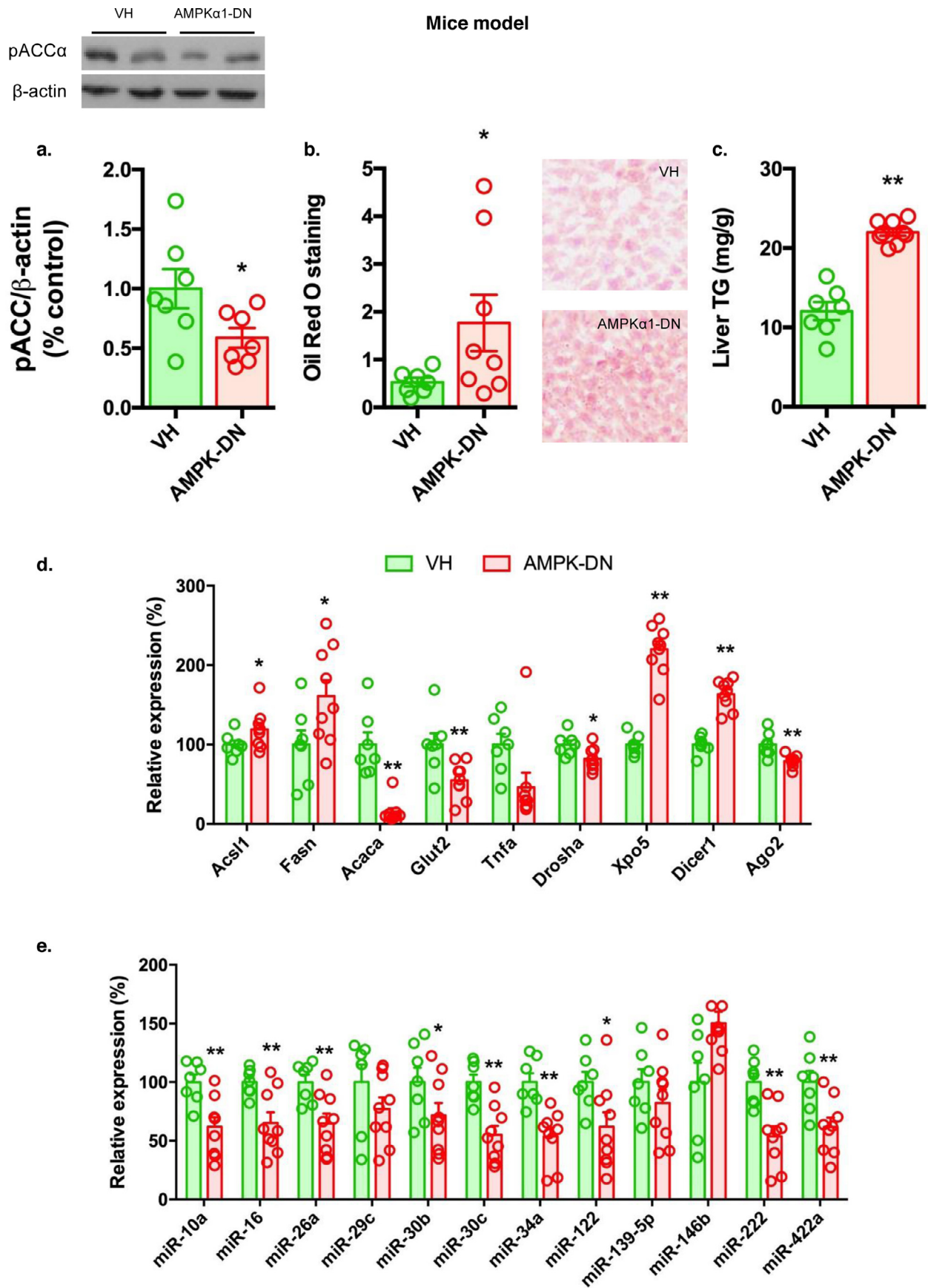
Fig. 4. Impact of hepatic *AMPK* knockdown *in vivo*. **a)** Hepatic levels of phospho(p)-ACC protein levels normalized by β-actin. **b)** Oil Red O stained area in liver samples, and **c)** milligrams of triglyceride (TG) content normalized by grams of tissue. **d)** Gene and **e)** miRNA expression in mice subjected to tail-injection of AMPK sh-RNA lentivirus (AMPK-DN, *n* = 9) *vs* vehicle (VH, *n* = 7). Data is expressed as mean ± SEM (* *p*<0.05, ** *p*<0.01 [Student *t*-test]).
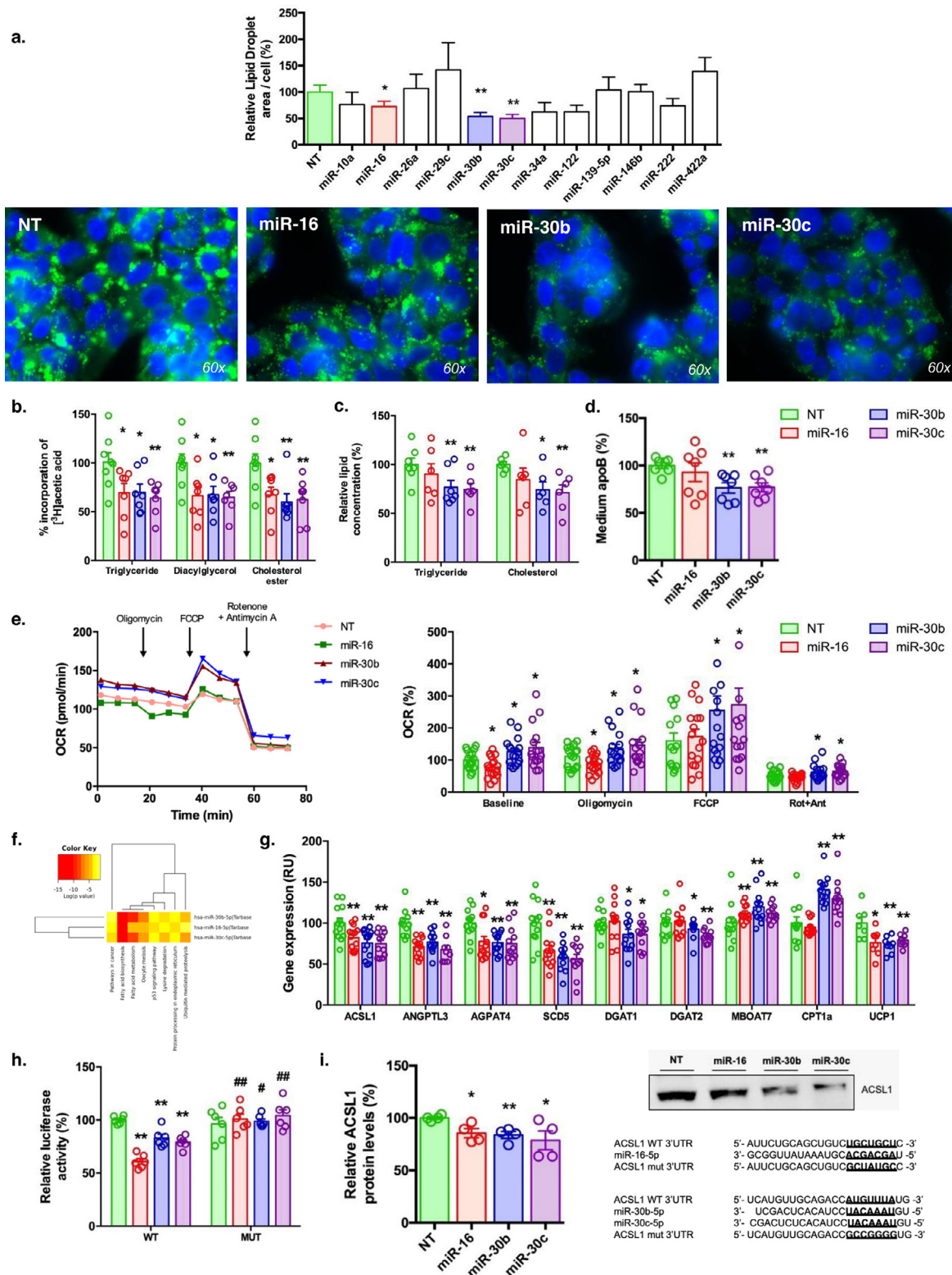
Fig. 5. Impact of miRNA candidates on lipid metabolism. **a)** Lipid droplet staining in Huh7 cells transfected with a non-targeting (NT) miRNA control and different mimic miRNA candidates. Bar plots show average of lipid droplet area *vs* cell number. Bodipy 493/503 (green) and DAPI (blue) report lipid droplets and nuclei, respectively. **b)** Triglyceride, diacylglycerol, and cholesterol esters (c.p.m. per ng protein) measured by thin-layer chromatography in HepG2 cells transfected with mimic miR-16, miR-30b, miR-30c, and NT miRNA control. **c)** Triglycerides and cholesterol content (mmol/ L per ng of protein) in culture supernatants. **d)** Apolipoprotein B (apoB) measures (ng/ μg cell protein). **e)** Oxygen consumption rate (OCR) in NT controls (orange dots), and HepG2 cells transfected with mimic miR-16 (green squares), miR-30b (straight red triangles), and miR-30c (inverted blue triangles). Seahorse quantification (pmol/ min/ μg protein) is shown in the plot. **f)** Heatmap showing predicted miRNA/ pathways clusters interaction, according to DIANA-miRPath v3.0 and TarBase v7.0. **g)** Expression of genes involved in lipid metabolism upon treatments with mimic miRNA candidates. **h)** Huh7 cells transfected with a wild-type control (WT) *ACSL1* 3'UTR dual Luc reporter and with mutated *ACSL1* 3'UTR (MUT). Firefly Luc activity normalized for *Renilla* signal is shown in plots. **i)** Western blot results for ACSL1 in HepG2 cells after transfection with NT miRNA control or mimic miRNA candidates (n = 4/ treatment). The ACSL1 signal was quantified and normalized against total protein. Complementary target region for *ACSL1* (WT and MUT) and miRNA candidates is also shown. Data in plots is expressed as mean ± SEM (* $p<0.05$, ** $p<0.01$ [One-Way ANOVA corrected by the Fisher's LSD test] for comparisons mimic *vs* NT miRNA control; # $p<0.05$, ## $p<0.01$ [Student *t*-test] for comparisons mutated *ACSL1* 3'UTR *vs* WT cells).

mitochondrial activity, we found an increase of carnitine palmitoyl-transferase 1 α (*CPT1α*) mRNA in cells treated with mimic miR-30b and miR-30c, while miR-16 did not impact its expression (Fig. 5g). On the other hand, 3′UTR binding sites for these miRNA candidates were identified in the gene coding for acyl-CoA synthetase long chain family member 1 (*ACSL1*). Thus, *ACSL1* 3′UTR luciferase reporter constructs were transfected into Huh7 cells, showing a significant reduction of the luciferase signal upon transfection with mimic miRNA candidates (Fig. 5h). Notably, luciferase activity was not modified in cells transfected with a mutated *ACSL1* 3′UTR reporter construct (Fig. 5h), hence confirming specific binding between current miRNA candidates and *ACSL1* mRNA. Finally, ACSL1 protein analysis endorsed the luciferase results, thus validating the causal relationship suggested by the complementary sequences (Fig. 5i).

3.7. Mimic miR-30b and miR-30c modulate the sphingomyelin/ceramide ratio

To obtain an overview of the effects accomplished by mimic miRNA transfections on the lipid profile, we subjected lipids extracted from human hepatocytes to quantitative direct flow injection electrospray ionization tandem mass spectrometry. Notably, PCA and heatmap analysis (Fig. 6a) discriminated the impact of mimic miR-16 from miR-30b and miR-30c. Consistent reduction of phosphatidylethanolamine plasmalogens and ceramides, together with an increase of sphingomyelins, were observed after the ectopic overexpression of miR-30b and miR-30c, the changes accomplished by miR-16 being less prominent (Fig. 6b). These findings were strongly supported by consistent changes in the expression of key enzymes related to the synthesis/degradation of sphingomyelins and ceramides, namely elevated sphingomyelin synthase 1 and 2 (*SGMS1* and *SGMS2*), and decreased sphingomyelin phosphodiesterase 2 (*SMPD2*) in hepatocytes transfected with mimic miR-30b or miR-30c (Fig. 6c). Noteworthy, the expression of genes involved in the formation and coating of lipid droplets (*PLIN1, SLC25A1,* and *MGAT1*) was also compromised by miR-30b and miR-30c, while miR-30b also reduced seipin (*BSCL2*) mRNA (Fig. 6c), an endoplasmic reticulum-resident protein of key importance in neutral lipid storage [43].

3.8. Recovery of miR-30b and miR-30c acts against FA accumulation in hepatocytes

As consistent downregulation of hepatic miR-30b and miR-30c was found in association with NAFLD and treatments that mimicked the onset of this condition [28], pointing the loss of these unique miRNA species at the forefront of the imbalance in hepatic lipid homeostasis, we wanted to see if their recovery restored lipid deposition after treatments triggering FA overload. As postulated, lipid droplet staining revealed the ability of miR-30b and miR-30c to reduce triglyceride storage in hepatocytes treated with CC, or those submitted to the partial knockdown of *AMPK* and *DICER* (Fig. 7a). Indeed, replenishment of miR-30b and miR-30c (*i.e.* fold changes of 100−200 *versus* NT miRNA control) in hepatocytes with impaired *AMPK* or *DICER* activity, and also treatments with either mimic miR-30b and miR-30c on HepG2 cells challenged with CC, significantly reduced the lipid droplet area (Fig. 7b). In concordance, transfection of mimic miR-30b and miR-30c decreased the expression of *ACSL1* and *FASN* (Fig. 7c), and elevated *GLUT2* mRNA in human hepatocytes with impaired *AMPK* expression, suggestive of the partial restoration of glucose intake in this cell model. Also of a great interest, it should be noted that replenishment of miR-30b and miR-30c let to the increased expression of *CPT1α* (all models) and Peroxisome proliferator-activated receptor alpha (*PPARα*) (only in hepatocytes with defective *DICER*) (Fig. 7c), and thus may ameliorate β-oxidation impairment in *AMPK* and *DICER* knockdown HepG2 cells, as well as in hepatocytes treated with compounds that compromise AMPK activity.

3.9. Expression of hepatic miR-30b and miR-30c is associated with hepatosteatosis

With regard to the clinical relevance of the results explained above, real time PCR performed in liver samples from obese women with or without significant hepatosteatosis (*i.e.* fat content in liver >33%) confirmed significant downregulation in miR-16, miR-30b and miR-30c, together with increased *ACSL1* mRNA, and decreased *DICER* and *AMPK* in subjects with NAFLD (Fig. 8a). Indeed, *DICER* and *AMPK* gene expression levels in such liver biopsies were positive and significantly associated with current miRNA candidates (Fig. 8b). Moreover, the quantities of these three miRNAs were inversely correlated with body mass index and that of miR-30b with fasting triglycerides (Fig. 8b), further emphasizing their potential relevance as novel candidates to control fatty liver through the restauration of lipid homeostasis.

4. Discussion

Non-alcoholic fatty liver disease (NAFLD) is the main consequence of long-lasting metabolic impairment affecting hepatic *de novo* lipogenesis and fatty acid (FA) uptake, together with the inability to oxidize lipids that are gradually accumulated in hepatocytes [44]. Nowadays it is widely recognized that many of these procedures are mainly regulated by AMPK function [45−47]. Current findings highlight the apparent contribution of AMPK also to hepatic miRNA biosynthesis by means of its pharmacological modification and genetic blockade, accomplished both *in vitro* and *in vivo*. Indeed, as metformin [48] and compound C [49] have been postulated to trigger off-target effects, due to their ability to impact a broad variety of kinases that appear to be mediated by attenuation of biosynthetic and oxidative fluxes, lentiviral particles mediating specific AMPKα1/2 knockdown were employed. This confirmed, among others, miRNA downregulation as a result of diminished AMPK performance and impaired lipid homeostasis in human hepatocytes.

We next postulated that AMPK may regulate FA metabolism through miRNA availability. Accordingly, the interplay between AMPK and hepatic miRNA profiles leading to changes in FA metabolism was sustained by i) reduced AMPK activity/ expression coupled to decreased miRNA abundance and expression of genes related to miRNA biosynthesis, namely *DICER* and *DROSHA* under conditions mimicking the onset of NAFLD, ii) consistent decrease of miRNA candidates coinciding with increased FA accumulation, and iii) the ectopic replenishment of hepatic miR-30b and miR-30c, rescuing FA overload and modifying lipid profiles in human hepatocytes. In agreement, partial knockdown of *DICER* demonstrated that its downregulation is intrinsically coupled to significant changes in miRNA profiles and increased FA overload. This piece of data matches with previous studies reporting the interplay between DICER and miRNA profiles, controlling the epithelial-mesenchymal transition during oncogenic events [50], and increased DICER after treatments that modulate AMPK activity in both mice and humans [51,52]. Additionally, previous research performed in a dietary-induced NASH mouse model reported a significant decrease of hepatic *Dicer* [53]. Strikingly, both *AMPK* and *DICER* knockdown resulted in increased FA deposition in hepatocytes, which was partially counteracted by rescue of the diminished expression of two of the miRNA species most consistently affected, the miR-30b and miR-30c.

Variations in specific hepatic miRNA have been previously associated with NAFLD and lipid homeostasis [54−58]. Consistent results were reported with regard to miR-30c, which showed decreased expression in the liver of a leptin receptor-deficient mouse model [59], and in plasma from subjects with NAFLD [60]. miR-30c has been linked to lipid metabolism, disclosing its ability to dampen lipid biosynthesis and lipoprotein secretion, being postulated as a potential target against hyperlipidemia and related diseases [61,62]. Noteworthy, *in silico* prediction categorized genes related to *de novo*
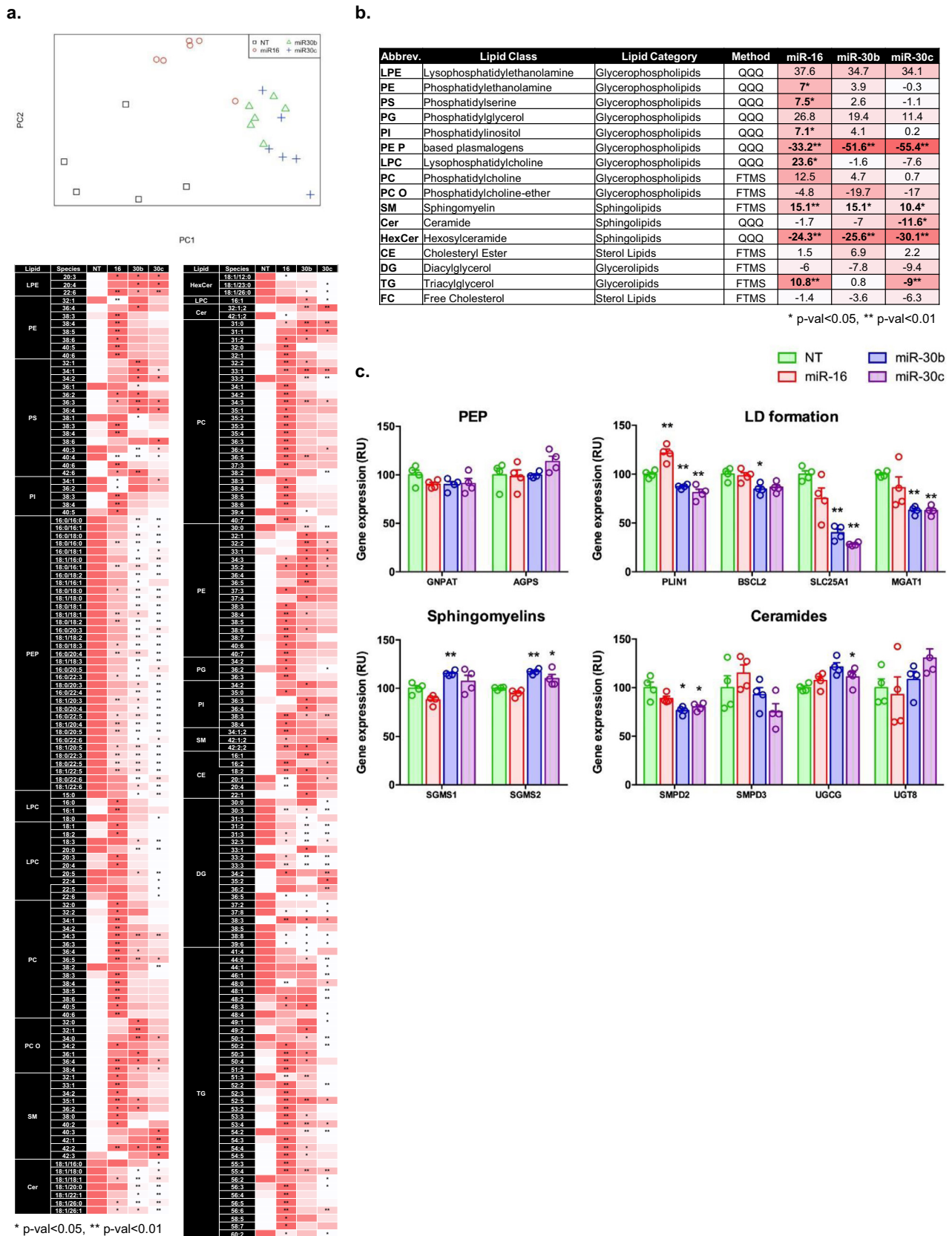
Fig. 6. Impact of mimic miR-16, miR-30b and miR-30c on lipid species. **a)** Principal component analysis (PCA) of lipid classes and families affected by treatments of a non-targeting (NT) miRNA control and mimic miRNA candidates in HepG2 cells. The intensity of red color-scale indicates relative presence of each lipid. **b)** Lipid species grouped in families significantly affected by mimic miR-16, miR-30b, and/or miR-30c. **c)** Expression of genes related to the synthesis and degradation of phosphatidylethanolamine plasmalogens (PEP), sphingomyelins and ceramides, and those associated with the formation of lipid droplets (LD). Data is expressed as mean ± SEM (*n* = 4 replicates/ treatment, * *p* < 0.05, ** *p* < 0.01 [One-Way ANOVA corrected by the Fisher's LSD test]).
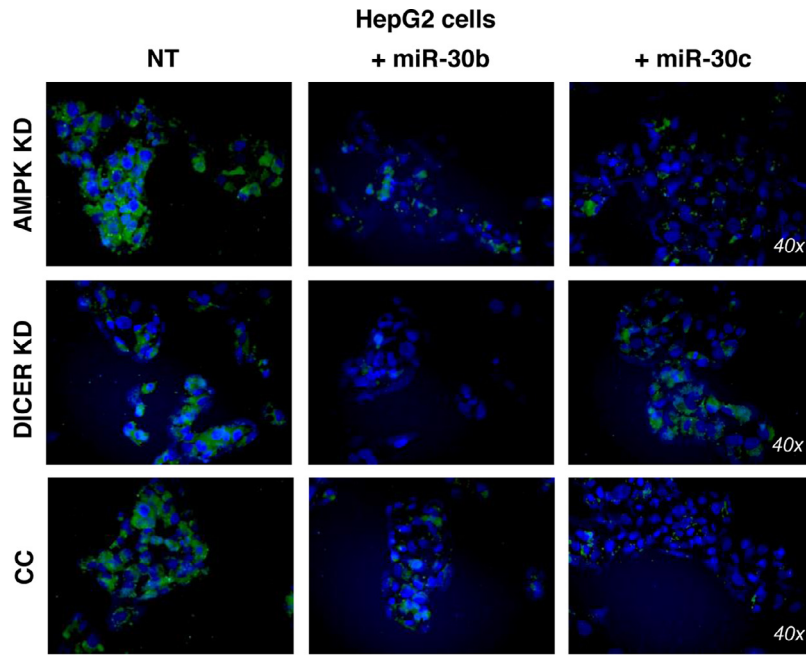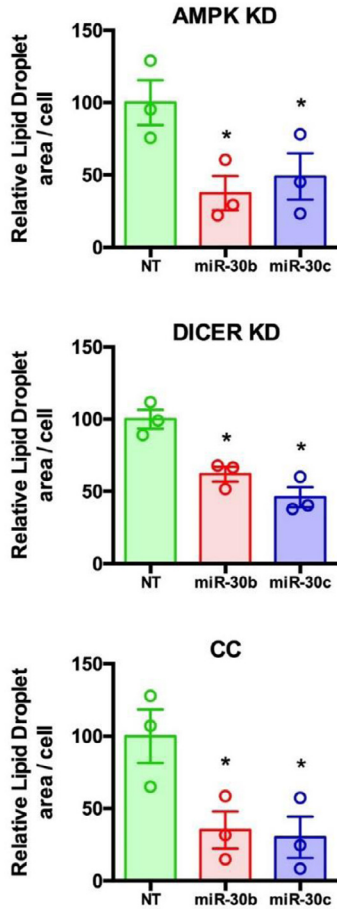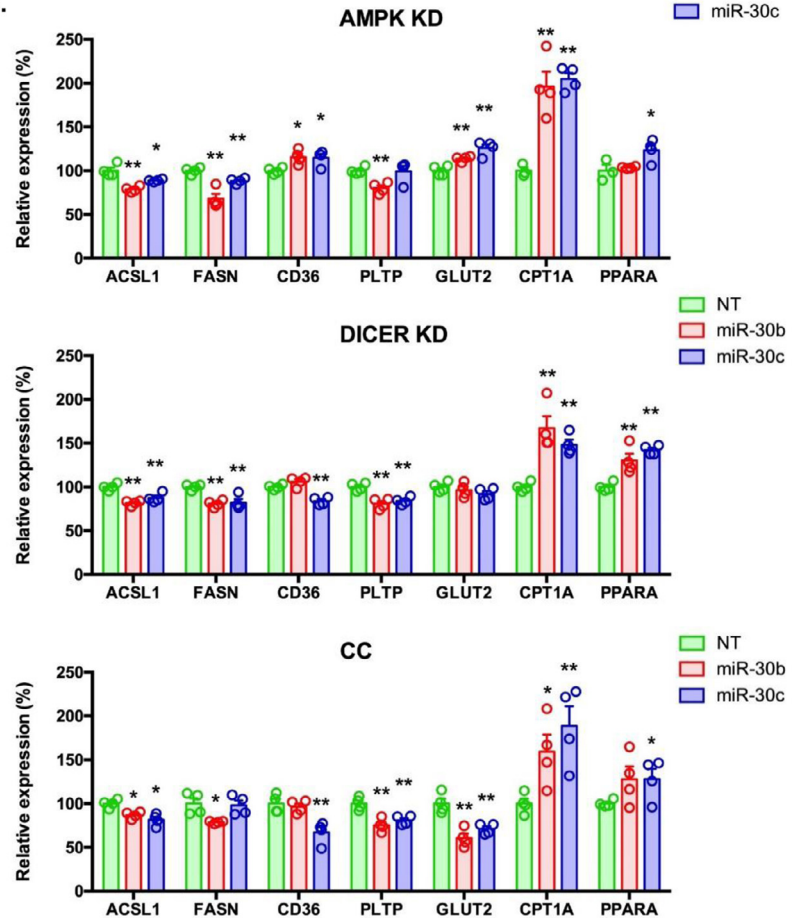
Fig. 7. Ectopic recovery of miR-30b and miR-30c protects against steatosis. **a)** Lipid droplet staining in HepG2 cells transfected with non-targeting (NT) control miRNA, miR-30b and miR-30c. Bodipy 493/503 (green) and DAPI (blue) report lipid droplets and nuclei, respectively. **b)** Bar plots represent relative lipid droplet area per cell area, the value for NT cells set at 100 ($n = 3$ replicates/ model/ treatment). **c)** Expression of genes related to FA biosynthesis, glucose intake, and β-oxidation after mimic transfection in treatments leading to increased FA deposition (*i.e. AMPK* and *DICER* knockdown (KD), and cells challenged with CC; $n = 4$ replicates/ model/ treatment). Data is expressed as mean $\pm$ SEM (* $p < 0.05$, ** $p < 0.01$ [One-Way ANOVA corrected by the Fisher's LSD test]).
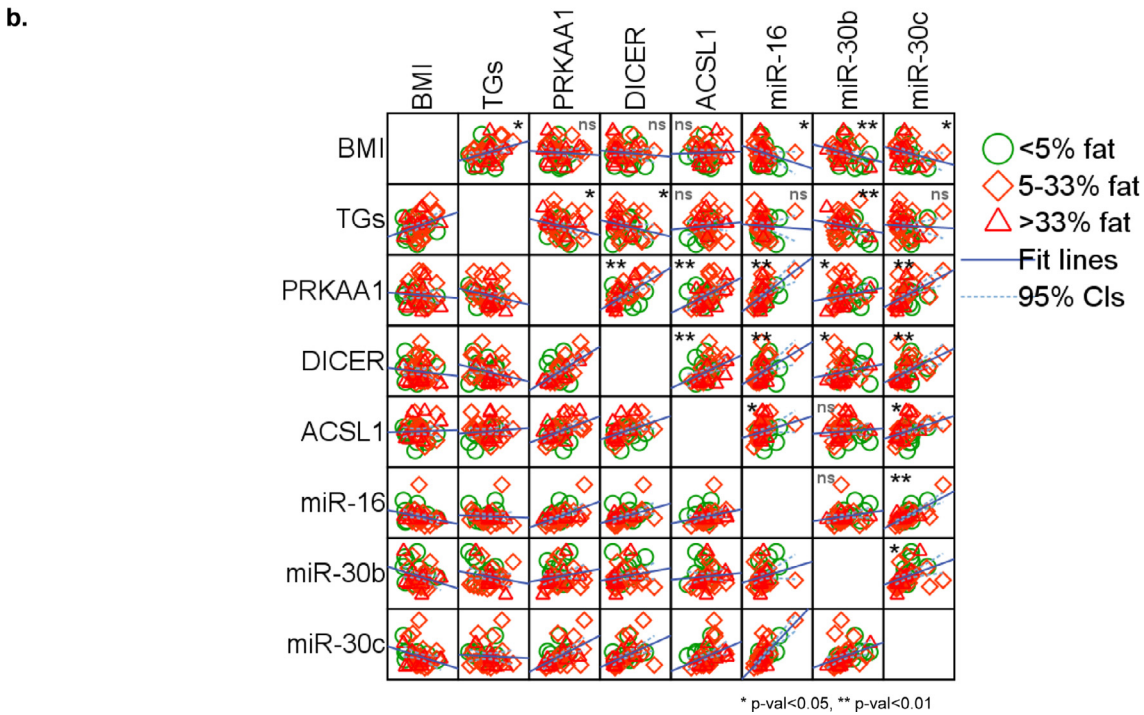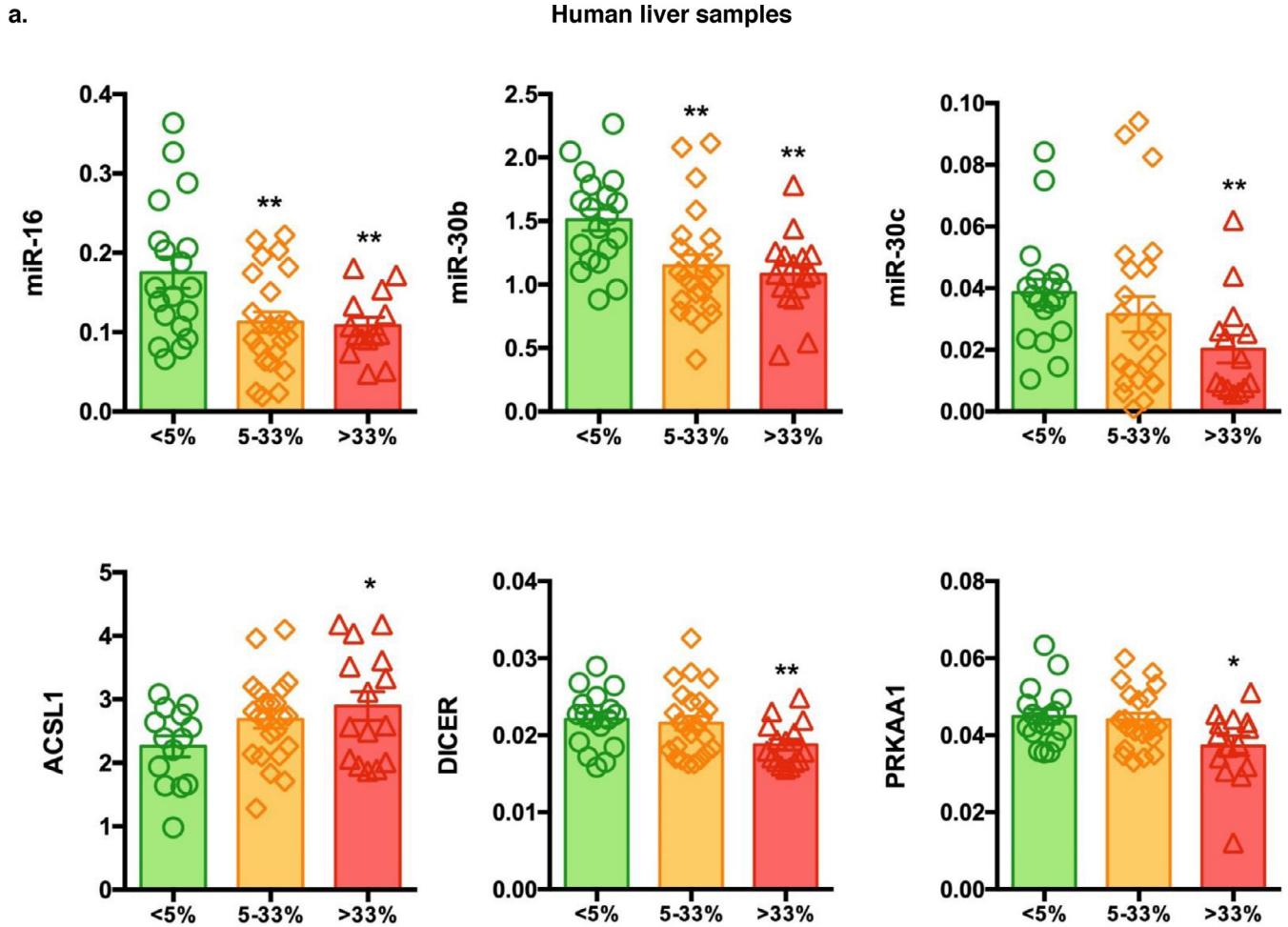
Fig. 8. Gene and hepatic miRNA expression in subjects with different degrees of steatosis. **a)** Expression of *miR-16, miR-30b, miR-30c, ACSL1, DICER* and *AMPK* (a.k.a. *PRKAA1*) in liver samples of obese women with different degrees of hepatosteatosis. **b)** Spearmans' correlations between miRNA and gene expression levels, body mass index (BMI), and fasting triglycerides (TGs) (* $p<0.05$, ** $p<0.01$, ns not significant). Data in bar plots is expressed as mean ± SD (* $p<0.05$, ** $p<0.01$ [One-Way ANOVA corrected by the Fisher's LSD test]).

lipogenesis and FA uptake as plausible targets for the differentially expressed miRNA candidates (Fig. 5f). The overall outcome of their downregulation under conditions mimicking steatosis (*i.e.* those accomplished through defective AMPK function, and by pathophysiological concentrations of saturated FA in the media, also characterized by decreased AMPK activity, Fig. 1) would be translated into decreased expression of miRNA candidates and the disability to actively repress specific target genes. As a consequence, this may result in impaired expression patterns, anomalous lipid metabolism, and the acquisition of NAFLD traits.

Specifically, miR-16, miR-30b and miR-30c were consistently involved in lipid homeostasis, as demonstrated by studies assessing organelle structure, gene expression, mitochondrial function, and mass spectrometric analysis of the hepatocyte lipidome. Thereby, replenishment of these miRNA candidates led to i) decreased lipid droplet accumulation, ii) impaired expression of genes related to the synthesis of triglycerides, and iii), in the case of mimic miR-30b and miR-30c, enhanced mitochondrial function coupled with increased $CPT1\alpha$ expression and modulation of genes related to the lipidome. Accordingly, $ACSL1$ was validated as a direct target, which is known to dynamically drive FA metabolism in hepatocytes [63]. Indeed, previous research suggested that $ACSL1$ channels radiolabeled oleate towards diacylglycerol, phosphatidyl-ethanolamine, phosphatidylinositol, and phosphatidylcholine, diminishing cholesterol esterification [64,65]. On the contrary, ACSL1 deficiency led to reduced FA biosynthesis and enabled β-oxidation [66]. Our results point out the higher expression of hepatic $ACSL1$ in NAFLD patients and under conditions mimicking enhanced FA deposition and decreased miRNA expression in hepatocytes, while the control exercised by miR-30b and miR-30c was coupled to increased mitochondrial function and decreased *de novo* lipogenesis.

Finally, lipidome-wide quantitative assessment shortlisted key differences between the activity exercised by mimic miR-16, miR-30b, and miR-30c, and a reduction of ceramides coinciding with an elevation of sphingomyelins, accomplished by miR-30b and miR-30c but not by miR-16. It should be noted that an increase in hepatic ceramides is associated with steatosis and insulin resistance [67], and that ACSL1 can induce excess synthesis of total acyl derived long chain ceramides [68], thus reinforcing the causal implications of our current results. On the other hand, sphingomyelins have been reported to attenuate hepatic steatosis in high-fat-diet-induced obese mice, proving beneficial effects [69]. Hence, the analysis of the lipidome in hepatocytes challenged with mimic miRNA candidates reinforced the potential therapeutic utility of the ectopic recovery of miR-30b and miR-30c in the fatty liver arena, restoring lipid homeostasis in human hepatocytes. Altogether, our data unravel the activity of miR-30b and miR-30c in tackling inadequate FA accumulation, offering a potential avenue for the treatment of NAFLD.

Declaration of competing interest

We certify that there is no conflict of interest to disclose regarding the materials and data discussed in this manuscript. The contents of this manuscript have not been copyrighted or published previously. There are no directly related manuscripts or abstracts, published or unpublished, by one or more authors of this manuscript. The submitted manuscript nor any similar script, in whole or in part, will be neither copyrighted, submitted, or published elsewhere while the Journal is under consideration.

Acknowledgments

Author contributions

JL, FJO designed the experiments, analysed biochemical variables, performed the statistical analysis, and wrote the manuscript. JMM-N, AL, FC, NO—C analysed biochemical variables and assisted with the setup of *in vitro* experiments. MH, YZ, GL, NHP, VO contributed to the performance and analyses of experiments, including lipidomics. LL-P, ML performed animal husbandry maintenance, treatment and characterization. WR, JMF-R obtained liver samples, clinical outputs, and the written consent of participants following bariatric surgery. VO, ML, JMF-R planned some of the experiments, revised the manuscript, and provided intellectual input.

Supplementary materials

Supplementary material associated with this article can be found in the online version at doi:10.1016/j.ebiom.2020.102697.

References

[1] Loomba R, Sanyal AJ. The global NAFLD epidemic. Nat Rev Gastroenterol Hepatol 2013. doi: 10.1038/nrgastro.2013.171.

[2] Brunt EM, Wong VW-S, Nobili V, Day CP, Sookoian S, Maher JJ, et al. Nonalcoholic fatty liver disease. Nat Rev Dis Prim 2015;1:15080.

[3] Byrne CD, Targher G. NAFLD: a multisystem disease. J Hepatol 2015. doi: 10.1016/j.jhep.2014.12.012.

[4] Yki-Järvinen H. Non-alcoholic fatty liver disease as a cause and a consequence of metabolic syndrome. Lancet Diabetes Endocrinol 2014;2:901–10. doi: 10.1016/S2213-8587(14)70032-4.

[5] Marchesini G, Brizi M, Bianchi G, Tomassetti S, Bugianesi E, Lenzi M, et al. Nonalcoholic fatty liver disease: a feature of the metabolic syndrome. Diabetes 2001. doi: 10.2337/diabetes.50.8.1844.

[6] Than NN, Newsome PN. A concise review of non-alcoholic fatty liver disease. Atherosclerosis 2015;239:192–202. doi: 10.1016/j.atherosclerosis.2015.01.001.

[7] Mansouri A, Gattolliat CH, Asselah T. Mitochondrial dysfunction and signaling in chronic liver diseases. Gastroenterology 2018. doi: 10.1053/j.gastro.2018.06.083.

[8] Sanders FWB, Griffin JL. De novo lipogenesis in the liver in health and disease: more than just a shunting yard for glucose. Biol Rev 2016. doi: 10.1111/brv.12178.

[9] Gan L, Xiang W, Xie B, Yu L. Molecular mechanisms of fatty liver in obesity. Front Med 2015;9:275–87. doi: 10.1007/s11684-015-0410-2.

[10] Li Y, Xu S, Mihaylova MM, Zheng B, Hou X, Jiang B, et al. AMPK phosphorylates and inhibits SREBP activity to attenuate hepatic steatosis and atherosclerosis in diet-induced insulin-resistant mice. Cell Metab 2011;13:376–88. doi: 10.1016/j.cmet.2011.03.009.

[11] Day EA, Ford RJ, Steinberg GR. AMPK as a therapeutic target for treating metabolic diseases. Trends Endocrinol Metab 2017;28:545–60. doi: 10.1016/j.tem.2017.05.004.

[12] Smith BK, Marcinko K, Desjardins EM, Lally JS, Ford RJ, Steinberg GR. Treatment of nonalcoholic fatty liver disease: role of AMPK. Am J Physiol - Endocrinol Metab 2016;311. doi: 10.1152/ajpendo.00225.2016.

[13] Esquejo RM, Salatto CT, Delmore J, Albuquerque B, Reyes A, Shi Y, et al. Activation of liver AMPK with PF-06409577 corrects NAFLD and lowers cholesterol in rodent and primate preclinical models. EBioMedicine 2018. doi: 10.1016/j.ebiom.2018.04.009.

[14] Lin HZ, Yang SQ, Chuckaree C, Kuhajda F, Ronnet G, Diehl AM. Metformin reverses fatty liver disease in obese, leptin-deficient mice. Nat Med 2000. doi: 10.1038/79697.

[15] Zhou G, Myers R, Li Y, Chen Y, Shen X, Fenyk-Melody J, et al. Role of AMP-activated protein kinase in mechanism of metformin action. J Clin Invest 2001. doi: 10.1172/JCI13505.

[16] Fullerton MD, Galic S, Marcinko K, Sikkema S, Pulinilkunnil T, Chen ZP, et al. Single phosphorylation sites in ACC1 and ACC2 regulate lipid homeostasis and the insulin-sensitizing effects of metformin. Nat Med 2013. doi: 10.1038/nm.3372.

[17] Boudaba N, Marion A, Huet C, Pierre R, Viollet B, Foretz M. AMPK re-activation suppresses hepatic steatosis but its downregulation does not promote fatty liver development. EBioMedicine 2018. doi: 10.1016/j.ebiom.2018.01.008.

[18] You M, Matsumoto M, Pacold CM, Cho WK, Crabb DW. The role of AMP-activated protein kinase in the action of ethanol in the liver. Gastroenterology 2004. doi: 10.1053/j.gastro.2004.09.049.

[19] Isakovic A, Harhaji L, Stevanovic D, Markovic Z, Sumarac-Dumanovic M, Starcevic V, et al. Dual antiglioma action of metformin: cell cycle arrest and mitochondria-dependent apoptosis. Cell Mol Life Sci 2007. doi: 10.1007/s00018-007-7080-4.

[20] Tang YC, Williams BR, Siegel JJ, Amon A. Identification of aneuploidy-selective antiproliferation compounds. Cell 2011. doi: 10.1016/j.cell.2011.01.017.

[21] Joshi-Barve S, Barve SS, Amancherla K, Gobejishvili L, Hill D, Cave M, et al. Palmitic acid induces production of proinflammatory cytokine interleukin-8 from hepatocytes. Hepatology 2007. doi: 10.1002/hep.21752.

[22] Friedman SL, Neuschwander-Tetri BA, Rinella M, Sanyal AJ. Mechanisms of NAFLD development and therapeutic strategies. Nat Med 2018. doi: 10.1038/s41591-018-0104-9.

[23] Baek D, Villén J, Shin C, Camargo FD, Gygi SP, Bartel DP. The impact of microRNAs on protein output. Nature 2008. doi: 10.1038/nature07242.

[24] Lim LP, Lau NC, Garrett-Engele P, Grimson A, Schelter JM, Castle J, et al. Microarray analysis shows that some microRNAs downregulate large numbers of-target mRNAs. Nature 2005. doi: 10.1038/nature03315.

[25] Selbach M, Schwanhäusser B, Thierfelder N, Fang Z, Khanin R, Rajewsky N. Widespread changes in protein synthesis induced by microRNAs. Nature 2008. doi: 10.1038/nature07228.

[26] Ferreira DMS, Simão AL, Rodrigues CMP, Castro RE. Revisiting the metabolic syndrome and paving the way for microRNAs in non-alcoholic fatty liver disease. FEBS J 2014;281:2503–24. doi: 10.1111/febs.12806.

[27] Baffy G. MicroRNAs in nonalcoholic fatty liver disease. J Clin Med 2015;4:1977–88. doi: 10.3390/jcm4121953.

[28] Latorre J, Moreno-Navarrete JM, Mercader JM, Sabater M, Rovira Ò, Gironès J, et al. Decreased lipid metabolism but increased FA biosynthesis are coupled with changes in liver microRNAs in obese subjects with nafld. Int J Obes 2017;41:620–30. doi: 10.1038/ijo.2017.21.

[29] Aguilo F, Zhang F, Sancho A, Fidalgo M, Di Cecilia S, Vashisht A, et al. Coordination of m6A mRNA methylation and gene transcription by ZFP217 regulates pluripotency and reprogramming. Cell Stem Cell 2015;17:689–704. doi: 10.1016/j.stem.2015.09.005.

[30] Ortega FJ, Moreno M, Mercader JM, Moreno-Navarrete JM, Fuentes-Batllevell N, Sabater M, et al. Inflammation triggers specific microRNA profiles in human adipocytes and macrophages and in their supernatants. Clin Epigenetics 2015;7. doi: 10.1186/s13148-015-0083-3.

[31] Ruhanen H, Nidhina Haridas PA, Eskelinen EL, Eriksson O, Olkkonen VM, Käkelä R. Depletion of TM6SF2 disturbs membrane lipid composition and dynamics in HUH7 hepatoma cells. Biochim Biophys Acta - Mol Cell Biol Lipids 2017;1862:676–85. doi: 10.1016/j.bbalip.2017.04.004.

[32] Bligh EG, Dyer WJ. A rapid method of total lipid extraction. Can J Biochem Physiol 1959;37:911–7. doi: 10.1145/3163918.

[33] Liebisch G, Lieser B, Rathenberg J, Drobnik W, Schmitz G. High-throughput quantification of phosphatidylcholine and sphingomyelin by electrospray ionization tandem mass spectrometry coupled with isotope correction algorithm. Biochim Biophys Acta - Mol Cell Biol Lipids 2004;1686:108–17. doi: 10.1016/j.bbalip.2004.09.003.

[34] Liebisch G, Binder M, Schifferer R, Langmann T, Schulz B, Schmitz G. High throughput quantification of cholesterol and cholesteryl ester by electrospray ionization tandem mass spectrometry (ESI-MS/MS). Biochim Biophys Acta - Mol Cell Biol Lipids 2006;1761:121–8. doi: 10.1016/j.bbalip.2005.12.007.

[35] Höring M, Ejsing CS, Hermansson M, Liebisch G. Quantification of cholesterol and cholesteryl ester by direct flow injection high resolution FTMS utilizing species-specific response factors. Anal Chem 2019. doi: 10.1021/acs.analchem.8b05013.

[36] Liebisch G, Vizcaino JA, Koefeler H, Troetzmueller M, Griffiths WJ, Schmitz G, et al. Shorthand notation for lipid structures derived from mass spectrometry. J Lipid Res 2013;54. doi: 10.1194/jlr.M033506.

[37] Husen P, Tarasov K, Katafiasz M, Sokol E, Vogt J, Baumgart J, et al. Analysis of lipid experiments (ALEX): a software framework for analysis of high-resolution shotgun lipidomics data. PLoS One 2013;8. doi: 10.1371/journal.pone.0079736.

[38] Latorre J., Ortega F.J., Liñares-Pose L., Moreno-Navarrete J.-.M., Lluch A., Comas F., et al. miRNAlipidomics.zip2020. doi:10.6084/m9.figshare.11854563.v1.

[39] Vlachos IS, Zagganas K, Paraskevopoulou MD, Georgakilas G, Karagkouni D, Vergoulis T, et al. DIANA-miRPath v3.0: deciphering microRNA function with experimental support. Nucl Acids Res 2015. doi: 10.1093/nar/gkv403.

[40] Huang DW, Sherman BT, Lempicki RA. Bioinformatics enrichment tools: paths toward the comprehensive functional analysis of large gene lists. Nucl Acids Res 2009;37:1–13. doi: 10.1093/nar/gkn923.

[41] Kersten S. Angiopoietin-like 3 in lipoprotein metabolism. Nat Rev Endocrinol 2017. doi: 10.1038/nrendo.2017.119.

[42] Eslam M, Valenti L, Romeo S. Genetics and epigenetics of NAFLD and NASH: clinical impact. J Hepatol 2018. doi: 10.1016/j.jhep.2017.09.003.

[43] Salo VT, Belevich I, Li S, Karhinen L, Vihinen H, Vigouroux C, et al. Seipin regulates ER−lipid droplet contacts and cargo delivery. EMBO J 2016. doi: 10.15252/embj.201695170.

[44] Ferré P, Foufelle F. Hepatic steatosis: a role for de novo lipogenesis and the transcription factor SREBP-1c. Diabetes, Obes Metab 2010;12:83–92. doi: 10.1111/j.1463-1326.2010.01275.x.

[45] Garcia D, Shaw RJ. AMPK: mechanisms of cellular energy sensing and restoration of metabolic balance. Mol Cell 2017;66:789–800. doi: 10.1016/j.molcel.2017.05.032.

[46] Woods A, Williams JR, Muckett PJ, Mayer FV, Liljevald M, Bohlooly YM, et al. Liver-Specific activation of AMPK prevents steatosis on a high-fructose diet. Cell Rep 2017;18:3043–51. doi: 10.1016/j.celrep.2017.03.011.

[47] Yao H, Tao X, Xu L, Qi Y, Yin L, Han X, et al. Dioscin alleviates non-alcoholic fatty liver disease through adjusting lipid metabolism via SIRT1/AMPK signaling pathway. Pharmacol Res 2018;131:51–60. doi: 10.1016/j.phrs.2018.03.017.

[48] Viollet B, Guigas B, Sanz Garcia N, Leclerc J, Foretz M, Andreelli F. Cellular and molecular mechanisms of metformin: an overview. Clin Sci 2012. doi: 10.1042/CS20110386.

[49] Cohen P, Plater L, Bain J, Klevernic I, Arthur JSC, Mclauchlan H, et al. The selectivity of protein kinase inhibitors: a further update. Biochem J 2008;408:297–315. doi: 10.1042/bj20070797.

[50] Martello G, Rosato A, Ferrari F, Manfrin A, Cordenonsi M, Dupont S, et al. A microRNA targeting dicer for metastasis control. Cell 2010;141:1195–207. doi: 10.1016/j.cell.2010.05.017.

[51] Noren Hooten N, Martin-Montalvo A, Dluzen DF, Zhang Y, Bernier M, Zonderman AB, et al. Metformin-mediated increase in DICER1 regulates microRNA expression and cellular senescence. Aging Cell 2016;15:572–81. doi: 10.1111/acel.12469.

[52] Blandino G, Valerio M, Cioce M, Mori F, Casadei L, Pulito C, et al. Metformin elicits anticancer effects through the sequential modulation of DICER and c-MYC. Nat Commun 2012;3. doi: 10.1038/ncomms1859.

[53] Liu MX, Gao M, Li CZ, Yu CZ, Yan H, Peng C, et al. Dicer1/miR-29/HMGCR axis contributes to hepatic free cholesterol accumulation in mouse non-alcoholic steatohepatitis. Acta Pharmacol Sin 2017;38:660–71. doi: 10.1038/aps.2016.158.

[54] Cheung O, Puri P, Eicken C, Contos MJ, Mirshahi F, Maher JW, et al. Nonalcoholic steatohepatitis is associated with altered hepatic microRNA expression. Hepatology 2008. doi: 10.1002/hep.22569.

[55] Du J, Niu X, Wang Y, Kong L, Wang R, Zhang Y, et al. MiR-146a-5p suppresses activation and proliferation of hepatic stellate cells in nonalcoholic fibrosing steatohepatitis through directly targeting Wnt1 and Wnt5a. Sci Rep 2015;5. doi: 10.1038/srep16163.

[56] Feng YY, Xu XQ, Ji CB, Shi CM, Guo XR, Fu JF. Aberrant hepatic microRNA expression in nonalcoholic fatty liver disease. Cell Physiol Biochem 2014;34:1983–97. doi: 10.1159/000366394.

[57] He Q, Li F, Li J, Li R, Zhan G, Li G, et al. MicroRNA-26a-interleukin (IL)-6-IL-17 axis regulates the development of non-alcoholic fatty liver disease in a murine model. Clin Exp Immunol 2017;187:174–84. doi: 10.1111/cei.12838.

[58] Cao P, Zhang Q, Wan M, Wang J, Wang Y, Zhang Q, et al. Fatty acid synthase is a primary target of mir-15a and mir-16-1 in breast cancer. Oncotarget 2016. doi: 10.18632/oncotarget.12479.

[59] Fan J, Li H, Nie X, Yin Z, Zhao Y, Chen C, et al. MiR-30c-5p ameliorates hepatic steatosis in leptin receptor-deficient (db/db) mice via down-regulating FASN. Oncotarget 2017;8:13450–63. doi: 10.18632/oncotarget.14561.

[60] Mehta R, Otgonsuren M, Younoszai Z, Allawi H, Raybuck B, Younossi Z. Circulating miRNA in patients with non-alcoholic fatty liver disease and coronary artery disease. BMJ Open Gastroenterol 2016;3:e000096. doi: 10.1136/bmjgast-2016-000096.

[61] Soh J, Iqbal J, Queiroz J, Fernandez-Hernando C, Hussain MM. MicroRNA-30c reduces hyperlipidemia and atherosclerosis in mice by decreasing lipid synthesis and lipoprotein secretion. Nat Med 2013;19:892–900. doi: 10.1038/nm.3200.

[62] Irani S, Hussain MM. Role of microRNA-30c in lipid metabolism, adipogenesis, cardiac remodeling and cancer. Curr Opin Lipidol 2015;26:139–46. doi: 10.1097/MOL.0000000000000162.

[63] Young PA, Senkal CE, Suchanek AL, Grevengoed TJ, Lin DD, Zhao L, et al. Long-chain acyl-CoA synthetase 1 interacts with key proteins that activate and direct fatty acids into niche hepatic pathways. J Biol Chem 2018. doi: 10.1074/jbc.RA118.004049.

[64] Li LO, Mashek DG, An J, Doughman SD, Newgard CB, Coleman RA. Overexpression of rat long chain acyl-CoA synthetase 1 alters fatty acid metabolism in rat primary hepatocytes. J Biol Chem 2006. doi: 10.1074/jbc.M604427200.

[65] Parkes HA, Carpenter L, Wood L, Ballesteros M, Furler SM, Kraegen EW, et al. Overexpression of acyl-CoA synthetase-1 increases lipid deposition in hepatic (HepG2) cells and rodent liver in vivo. Am J Physiol Metab 2006. doi: 10.1152/ajpendo.00112.2006.

[66] Li LO, Ellis JM, Paich HA, Wang S, Gong N, Altshuller G, et al. Liver-specific loss of long chain acyl-CoA synthetase-1 decreases triacylglycerol synthesis and β-oxidation and alters phospholipid fatty acid composition. J Biol Chem 2009. doi: 10.1074/jbc.M109.022467.

[67] Luukkonen PK, Zhou Y, Sädevirta S, Leivonen M, Arola J, Orešič M, et al. Hepatic ceramides dissociate steatosis and insulin resistance in patients with non-alcoholic fatty liver disease. J Hepatol 2016;64:1167–75. doi: 10.1016/j.jhep.2016.01.002.

[68] Goldenberg JR, Wang X, Lewandowski ED. Acyl CoA synthetase-1 links facilitated long chain fatty acid uptake to intracellular metabolic trafficking differently in hearts of male versus female mice. J Mol Cell Cardiol 2016;94:1–9. doi: 10.1016/j.yjmcc.2016.03.006.

[69] Norris GH, Porter CM, Jiang C, Millar CL, Blesso CN. Dietary sphingomyelin attenuates hepatic steatosis and adipose tissue inflammation in high-fat-diet-induced obese mice. J Nutr Biochem 2017. doi: 10.1016/j.jnutbio.2016.09.017.